IEEE Transactions on Automation Science and Engineering (T-ASE) paper, presented at ICRA 2026, Vienna, Austria.
Cite as T-ASE paper.

A Stable Model Reference Adaptive Controller Developed for a Prosthetic Hand Wrist

Shifa Sulaiman[1], Paolino De Risi[2], Francesco Schetter[3], and Fanny Ficuciello[4]

***Abstract*—Advanced control algorithms are essential for enhancing the functionality of prosthetic hands, enabling them to operate in diverse conditions. This paper presents a Model Reference Adaptive Controller (MRAC) developed for a tendon-driven soft continuum wrist, integrated into the 'PRISMA HAND II' prosthetic hand. The primary objective of our research is to design an adaptive controller that facilitates wrist movements eliminating external disturbances while minimizing computational requirements. To achieve this, kinematic and dynamic models of the wrist are developed based on the Piece-wise Constant Curvature (PCC) hypothesis. The controller consists of a reference model generated using the PCC model, and state errors are evaluated by comparing the responses of the reference model to those of the wrist model. These errors are reduced using the MRAC approach to make the wrist's behavior closely align with that of the reference model. Stability of the closed-loop system is ensured using the Lyapunov direct method, along with the 'New Theorem of Stability', a replacement for Barbalat's lemma, ensuring that the error between the reference model and the actual system converges to zero and that the adaptive gains stabilize to fixed values. The adaptive performance of the controller is evaluated through experimental validations, where the motions of the prosthetic hand attached to the wrist are treated as unknown disturbances, and the mechanical stiffness of the wrist is considered as an uncertain parameter, resulting from the degradation of the internal springs.**

Note to Practitioners - **This study aims to develop an adaptive controller suitable for soft continuum robots operating in diverse environments and conditions. Implementation of the proposed controller will enable soft robots to operate effectively in the presence of unknown disturbances.**

***Index Terms*—Model reference adaptive controller, Piece-wise Constant Curvature modelling, Prisma hand II, Dynamic modelling, Soft continuum wrist**

I. Introduction

CONTROL algorithms are integral to the operation of prosthetic hands, enhancing their ability to perform movements with greater precision and dexterity. These algorithms empower users with improved control, enabling them to engage more effectively in daily activities and tasks. The implementation of advanced control strategies not only enhances the performance of prosthetic hands but also contributes to an overall better user experience, increasing comfort and satisfaction for individuals who rely on these devices.

This work was supported by the Italian Ministry of Research under the complementary actions to the NRRP "Fit4MedRob - Fit for Medical Robotics" Grant (PNC0000007). All authors are from the Department of Information Technology and Electrical Engineering, Università degli Studi di Napoli Federico II, via Claudio 21, 80125 Napoli, Italy. [1]ssajmech@gmail.com, [2]paolino.derisi@unina.it, [3]schfrn@gmail.com, [4]fanny.ficuciello@unina.it

In control systems, the implementation of a Model Reference Adaptive Controller (MRAC) [1] is of significant importance [2]. This advanced control approach improves system performance by adapting to variations in system dynamics and external disturbances. By leveraging a reference model, the MRAC adjusts its parameters dynamically to ensure that the output of the controlled system closely follows the trajectory set by the reference model [3]. This adaptability is crucial in environments where system parameters are uncertain or subject to change over time.

The MRAC's key advantage lies in its ability to maintain optimal performance despite uncertainties and system variations, something traditional control methods often struggle to achieve. As the MRAC learns from the system's behavior, it makes necessary adjustments to control parameters, enhancing the system's robustness and reliability. This makes MRAC an ideal solution for applications ranging from aerospace to robotics. Furthermore, the MRAC contributes to greater efficiency in control systems by minimizing errors between the actual and desired outputs, which in turn reduces energy consumption from corrective actions. This efficiency is particularly important in applications where energy is limited or operational costs must be minimized.

In designing an effective control system for a prosthetic wrist, it is crucial to account for gravitational and dynamic effects that significantly influence its movement [4]. A kinematic model, which primarily considers geometric constraints and motion relationships, falls short in addressing these continuously changing forces. Gravity exerts variable torques depending on wrist orientation, introducing errors that a static model cannot compensate during the motion. Additionally, wrist movements generate inertia and velocity-dependent forces, impacting tendon-driven actuation and requiring real-time adjustments for precision control. Without incorporating these dynamic factors, the system would struggle to maintain stability during rapid motions. Thus, an adaptive control strategy, such as the MRAC, is employed to ensure robust compensation for these variations. By utilizing a dynamic model instead of a kinematic one, we enhance performance, improve trajectory tracking, and achieve more reliable functionality in practical applications.

This paper focuses on the design of an adaptive control system for a soft continuum wrist of a prosthetic hand. The system employs a model reference approach, allowing it to adjust its parameters during operation to accommodate dynamic changes in user movements and the external environment. This is achieved by integrating a model of the system derived from a Piece-wise Constant Curvature (PCC)

IEEE Transactions on Automation Science and Engineering (T-ASE) paper, presented at ICRA 2026, Vienna, Austria.

approach. By utilizing this model reference framework, the controller effectively emulates the desired behavior of a natural wrist, thereby improving the functionality and responsiveness of the prosthetic device. Additionally, we ensure the stability of the proposed control system using Lyapunov analysis, in conjunction with the 'New Theorem of Stability' proposed in [5], replacing the classic Barbalat's lemma. Our constructive proof demonstrates the convergence of state errors to zero and the stabilization of adaptive gains to fixed values, ensuring the effectiveness and reliability of the control system.

The development of an adaptive controller that offers fast dynamic response with minimal computational cost is crucial for improving wrist motion systems. Our research aims to optimize the trade-off between responsiveness and computational efficiency, ultimately enhancing the performance and reliability of wrist motion control systems. The goal is to provide a solution that meets the demands of real-world applications requiring efficient and precise control of wrist motions. We present a control strategy designed to leverage the motion of a soft continuum wrist, effectively compensating for the disruptive effects caused by the movement of an attached prosthetic hand, which acts as a gravitational disturbance. Our model also incorporates an uncertain parameter, the stiffness of the springs used in the soft wrist. Notably, the wear and degradation of these springs can lead to a deviation of the stiffness from its nominal value, introducing further uncertainty into the system. The major contributions of this work include:

- **MRAC formulation tailored to a tendon-driven PCC wrist with explicit disturbance-channeling and parametric degradation**: We introduce an MRAC that treats the prosthetic hand as a persistent gravitational disturbance and the wrist's spring stiffness as a time-varying, degrading parameter. The controller is structured to explicitly route both effects through the reference-tracking error, enabling online compensation without prior identification or disturbance observers.
- **Mapped soft-rigid dynamic bridge enabling lightweight control design**: We derive a four-element RPPR Denavit–Hartenberg parameterization that maps a PCC soft segment to an equivalent rigid–joint state-space model. This bridge allows us to derive closed-form mapped inertia, Coriolis/centrifugal, gravity, and tendon-force relationships and to synthesize an adaptive law on a reduced-order representation well-suited for embedded real-time execution.
- **Stability guarantee for configuration-dependent, time-varying soft-wrist dynamics using the New Theorem of Stability**: We extend MRAC stability analysis to a plant model whose matrices depend on configuration and time, proving convergence of both tracking errors and adaptive gains via a Lyapunov argument coupled with the New Theorem of Stability. This removes the uniform continuity requirement of Barbalat's lemma in the presence of disturbances and parameter drift, and to our knowledge provides the first such guarantee for a tendon-driven PCC wrist carrying a prosthetic hand.
- **Two reference-model alternatives that trade accuracy and effort, with a computationally efficient gain-update pathway**: We present and compare two scenarios - (I) a PD-controlled reference model with constant MRAC input, and (II) an open-loop reference model with time-varying MRAC input embedding PD action. We show that integrating the gain updates directly from the error dynamics (rather than repeatedly recomputing configuration-dependent matrices) preserves stability while substantially reducing online computation, enabling low-latency embedded control.
- **Degradation-aware design that is robust in practice, validated on the PRISMA HAND II wrist**: We embed a stiffness-degradation profile to capture wear-induced drift and show that residual unmodeled effects are handled adaptively. Experiments on the PRISMA HAND II wrist demonstrate fast gain convergence, disturbance rejection to external forces, and stable tracking under ±20% stiffness changes and increased payload confirming that the theoretical guarantees translate to a lightweight, real-time prosthetic system.

Collectively, these advances deliver a degradation-aware, disturbance-robust MRAC for a tendon-driven soft continuum wrist with a proof of stability tailored to configuration-dependent dynamics, a soft–rigid dynamic map that enables efficient implementation, and an experimentally validated pathway to practical embedded control.

The structure of this paper is as follows: Section II reviews previous literature on the development of MRAC for soft continuum mechanisms. Section III outlines the design and modeling procedures. Section IV details the MRAC strategy. Section V presents the stability analysis. Section VI provides simulation and experimental results. Finally, Section VII concludes the work.

II. Background

The MRAC strategy is applicable to a diverse range of robotic systems, encompassing both rigid [6] and soft robots [7]. MRAC control methodology is designed to enhance the motion control capabilities of robots, allowing for improved adaptability and precision in their movements. The adaptability of the MRAC framework allows for the continuous refinement of control laws, which is particularly beneficial in environments where external disturbances or changes in the operational context may occur.

Soft pneumatic actuators play a crucial role in enabling robots to engage safely with intricate environments [8]. However, they frequently encounter issues related to imprecise control and erratic dynamics [9]. Continell *et al.* [10] presented a hybrid control strategy for a tendon-driven soft robotic neck, aiming to achieve accurate pose control across its workspace. The work combined an analytical inverse kinematics model based on constant curvature assumptions with a Multi-Layer Perceptron (MLP) neural network that learned to correct pose errors using IMU sensor feedback. The research addressed the limitations of purely model-based approaches, which struggled with the nonlinearities of soft materials, and purely data-driven methods, which often lacked generalizability.

Seghiri *et al.* [11] introduced a fractional-order MRAC (FOMRAC) system for a single-degree-of-freedom flexible robotic arm, designed to maintain performance under varying payloads and joint friction. The control architecture featured a dual-loop design, an inner PID loop compensated for friction and coupling torque, while the outer loop used a fractional-order MIT adaptation law to handle payload changes and suppressed tip vibrations. The fractional calculus approach allowed for more accurate modeling of the system's dynamic behavior compared to traditional integer-order methods. Through simulation, the work demonstrated that the controller maintained stability and precision even under disturbances, addressing a key gap in adaptive control for flexible manipulators.

Huang *et al.* [12] proposed a hybrid modeling framework for soft parallel robots, combining the Absolute Nodal Coordinate Formulation (ANCF) with a multilayer neural network (MLNN). The ANCF model captured the quasi-static behavior of soft actuators, while the MLNN learned dynamic corrections, including viscoelastic effects and actuation hysteresis. This hybrid model was then used to design both feedforward and feedback-linearization controllers, enabling sub-millimeter tracking accuracy across a range of speeds. The approach was scalable, invertible, and suitable for real-time control, addressing the limitations of purely physics-based models (which were computationally intensive and less accurate under dynamic conditions) and purely data-driven models (which often lack interpretability).

An MRAC proposed in [13], illustrated a technique that adjusted an input to actuator parameters for ensuring its behavior aligned closely with a predetermined dynamic model. By utilizing adaptive control, the control scheme successfully normalized the performance of soft actuators and mitigated the inherent nonlinear characteristics. A hybrid control strategy that integrated a Proportional Integral Derivative (PID) controller with an MRAC applied to a manipulator was demonstrated in [14]. This approach employed the Lyapunov's theory to guarantee asymptotic stability during the control of a 2 degrees of freedom (DoF) manipulator, which was actuated by McKibben's artificial pneumatic muscles. In this framework, the MRAC functioned as a compensator for non-linearities, while the PID controller was utilized during the transient phase, as the performance of the MRAC was suboptimal in this specific period. Liu *et al.* [15] introduced a novel least-squares MRAC algorithm for multivariable systems. It modified the control law to reduce the relative degree of the error model to zero, enabling arbitrarily fast tracking while maintaining parameter convergence. The work provided a full Lyapunov-based stability analysis and demonstrate superior tracking performance through simulations.

An MRAC developed for a pneumatically actuated soft robot addressing system uncertainties by incorporating parametric variations and input limitations was presented in [16]. A soft robot was represented as a second-order Linear Parameter Varying (LPV) system, with the primary dynamics characterized as a Linear Time-Invariant (LTI) system. The design of the control scheme emphasized the significance of unidirectional input constraints. Additionally, adaptive laws were adjusted to mitigate the effects of parametric uncertainties and unmodeled dynamics. Licher *et al.* [17] presented an approach to control soft continuum robots by integrating MRAC with nonlinear Model Predictive Control (MPC). The method utilized a domain-decoupled physics-informed neural network (DD-PINN) trained on Cosserat rod dynamics to serve as a fast and accurate surrogate model. The controller adapted online using an unscented Kalman filter to estimate bending stiffness and internal states. The results showed real-time control at 70 Hz with sub-millimeter accuracy and significant computational speed-up compared to traditional physics-based simulations. However, the DD-PINN was trained offline, which can limit adaptability to unforeseen dynamic changes suggesting a future direction in online retraining or hybrid learning integration.

Zhou *et al.* [18] developed a bidirectional pneumatic artificial muscle (PAM) actuator for soft hand rehabilitation and implemented MRAC using a Radial Basis Function Neural Network (RBFNN). The system was modeled using Lagrangian mechanics and optimized for real-time control of grasping motions. The experiments demonstrated improved grip accuracy and responsiveness, particularly in stroke rehabilitation scenarios. While effective, the RBFNN controller required manual tuning and lacks generalization across different users, indicating a need for adaptive learning mechanisms that can personalize control based on individual EMG profiles.

Conventional controllers are generally developed based on the stability criterion stated by Lyapunov's 2nd method. However, Lyapunov criterion depends mostly on global stability and less focused on the tracking errors. A novel MRAC methodology (not based on Lyapunov function) named Robust Fixed Point Transformations (RFPT) employed during a master-slave task assignment was demonstrated in [19]. The proposed controller was able to simultaneously achieve adaptability and order reduction with less computational effort. Another novel dynamic model based MRAC strategy was presented in [20]. Similar to MRAC, Model Reference Predictive Adaptive Control (MRPAC) effectively addressed issues related to "parameter mismatch," including scenarios involving unknown inertia values. The findings indicated that MRPAC possessed the capability to adapt to these discrepancies, ensuring optimal performance even when certain parameters were not precisely defined or known. A study focused on the creation of a myoelectric MRAC integrated with an Adaptive Kalman filter, specifically designed for the regulation of a cable-driven soft elbow exoskeleton was given in [21]. The MRAC demonstrated its effectiveness in managing both passive and active control scenarios for the soft elbow exoskeleton. The performance metrics of the controlled system revealed a Mean Absolute Error (MAE) of approximately 4.5° in passive mode, while in active mode, the MAE was recorded around 10°.

Development of an adaptive force control strategy for soft robotic gripping, aiming to improve handling of delicate and irregularly shaped objects was demonstrated in [22]. A visual force sensor trained on synthetic data derived from finite element analysis (FEA) sensor was integrated with a nonlinear MRAC, forming a combined approach called virtual

IEEE Transactions on Automation Science and Engineering (T-ASE) paper, presented at ICRA 2026, Vienna, Austria.

reference adaptive control (VRAC). The VRAC strategy enabled effective force control while minimizing the complexity of integrating additional sensors, allowing the robotic gripper to adapt to different objects with minimal training.

Stability analysis is a crucial aspect of the design of MRAC, ensuring that the system behaves reliably and reaches desired states. A comprehensive review of various MRAC methodologies and their associated stability considerations is provided in [23]. One widely used technique for assessing stability in nonlinear systems is the direct Lyapunov method. This approach involves the formulation of a Lyapunov candidate function, $V(x)$, which must be positive definite, differentiable, and equal to zero only at the equilibrium point. For global asymptotic stability, it is necessary for the derivative, $\dot{V}(x,t)$, to be negative definite. However, deriving a Lyapunov function with a negative definite derivative can often be challenging, and in many cases, the derivative is only negative semi-definite. This necessitates generalizations of Lyapunov's direct method. In MRAC systems, which are typically non-autonomous and involve adaptive gains that vary over time, Barbalat's Lemma has been traditionally employed to demonstrate global asymptotic stability. However, Barbalat's Lemma requires that $\dot{V}(x,t)$ be uniformly continuous, a condition that also extends to all system signals. This requirement becomes problematic in the presence of disturbances or other discontinuities, which can disrupt the stability analysis, as highlighted in [24]. To overcome this limitation, a novel stability theorem was introduced in [5], which relaxed the uniform continuity condition. According to this theorem, for a non-autonomous nonlinear system with a Lyapunov candidate function $V(x)$ and a negative semi-definite derivative $\dot{V}(x,t)$, all limit points of any bounded trajectory $x(t)$ will lie within the domain $\Omega = x|\lim_{t\to\infty} \dot{V}(X,t) \equiv 0$, where $(\cdot) \equiv 0$ indicates that both the expression and its higher-order derivatives are zero. This generalized approach has proven effective in adaptive control applications, with examples provided in [25] that demonstrated the convergence of adaptive gains. Additionally, the theorem has been applied to the stability analysis of MRAC systems, including in [26], where it was used for an MRAC system with a time-invariant plant.

III. Design and Modelling of the Wrist

This section provides an overview of the components and mechanical design of the wrist integrated into the prosthetic hand. Additionally, the kinematic and dynamic modelings of the wrist, employing the PCC method for analysis are also included in this section.

A. Design of the Wrist

A soft continuum wrist section [28] was developed to integrate with a prosthetic hand named 'PRISMA HAND II' [8]. The final design of the wrist section was determined by evaluating its load-bearing capacity alongside its ability to facilitate movement in various directions, specifically ulnar, radial, flexion, and extension. The integration of the wrist with the PRISMA HAND II, along with the corresponding motion directions, is illustrated in Fig. 1(a). The fabricated

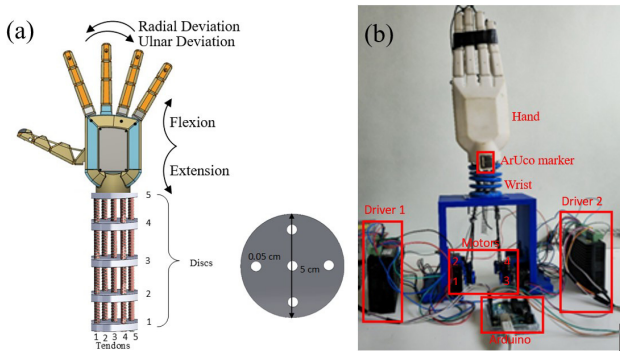

Fig. 1: Wrist section. (a) Conceptual model. (b) Fabricated model.

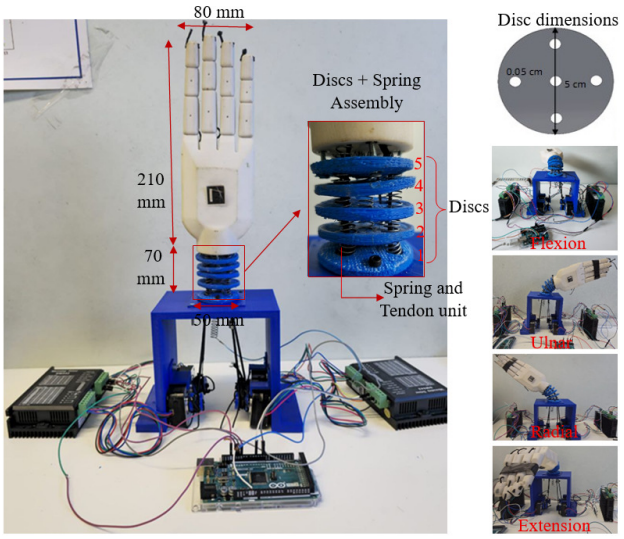

Fig. 2: Components of the fabricated model with dimensions and motion capabilities

wrist assembly (shown in Fig. 1(b)) consisted of 5 rigid discs, 5 springs, 5 tendons that were inserted through the springs, and 4 motors. The manipulation of these tendons using motors allowed for the execution of specific movements across various directions. Four peripheral tendons (shown in Fig. 1) connected to motors were employed to control rotational movements in four distinct directions. The dimensions of the components of the wrist along with the prosthetic hand motions are shown in Fig. 2. Tendons 1 and 2 were activated to induce wrist rotation in the radial deviation direction, while tendons 4 and 5 facilitated motion in the ulnar deviation direction. Extension movements were achieved by actuating tendons 1 and 4, whereas flexion was controlled through the actuation of tendons 2 and 5. In relation to disc 5, the wrist's range of motion was established to span from -50° to +50° across all axes as shown in Fig. 2. This configuration proved sufficient for the PRISMA HAND II to execute various manipulation tasks effectively. This configuration of components enabled the wrist section to also exhibit axial compression and expansion capabilities as shown in Fig. 3.

IEEE Transactions on Automation Science and Engineering (T-ASE) paper, presented at ICRA 2026, Vienna, Austria.

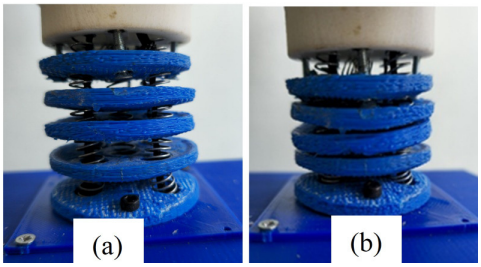

Fig. 3: Motion of wrist section in axial direction. (a) Initial stage. (b) Compressed stage.

B. Kinematic Modelling of the Wrist Using PCC Method

In the realm of soft robotics, the PCC model serves as a structured approach to comprehend the configuration of robots by dividing it into distinct segments that demonstrate continuous curvature (CC). This segmentation is essential, as it mitigates the inherent complexity associated with soft robots, which typically feature an infinite array of degrees of freedom with respect to their flexible structure. By utilizing a limited number of segments, the model not only improves computational efficiency but also facilitates a clearer and more intuitive description of the kinematic and dynamic behaviors of the robot.

Consider a soft continuum robot characterized by n continuous curves (CCs) as illustrated in Fig. 4(a). Fig. 4(a) visually conveys how motion propagates from one segment to the next, forming the basis for dynamic modeling and control strategies. It is essential to note that each segment of the robot is associated with frames represented as $S_0, S_1, ..., S_n$. These frames are systematically affixed to the terminal end of each segment, thereby facilitating a comprehensive understanding of the robot's configuration and movement dynamics. The transformation matrices that relate the n^{th} frame to the zeroth frame are denoted as ${}^0T_1, {}^1T_2, \ldots, {}^{n-1}T_n$. These matrices serve to describe the spatial relationships and orientations between consecutive frames.

A depiction of a single segment of the soft continuum robot is presented in Fig. 4(b). By isolating a single segment, the Fig. 4(b) helps to clarify the role of localized bending in the broader context of deformation transmission. It also supports the derivation of dynamic equations that govern the segment's behavior under actuation. This segment, located in the i^{th} plane, comprises two inertial reference frames positioned at its extremities, designated as S_{i-1} and S_i. The bending angles, denoted as θ_w, are derived from the analysis of the relative rotation occurring between these two inertial frames associated with the segment. The two-dimensional homogeneous transformation matrix for the soft robot, represented as ${}^{i-1}T_i$, which accounts for the section length l_i extending from the $(i-1)^{th}$ frame to the i^{th} frame within the i^{th} plane, is articulated in (1).

$$ {}^{i-1}T_i = \begin{bmatrix} cos\theta_w & -sin\theta_w & l_i\frac{sin\theta_w}{\theta_w} \\ sin\theta_w & cos\theta_w & l_i\frac{1-cos\theta_w}{\theta_w} \\ 0 & 0 & 1 \end{bmatrix}. \tag{1} $$

In this paper, we introduce a framework that demonstrates a correspondence between the modeling approaches of soft robots and rigid robots through the application of Denavit-Hartenberg (DH) parameterization [29]. This framework aims to bridge the gap between the two types of robotic systems, highlighting the similarities in their kinematic representations and providing a unified methodology for their analysis and design. By leveraging DH parameters, we can effectively characterize the motion and configuration of both soft and rigid robots, thereby enhancing our understanding of their operational dynamics and facilitating the development of more versatile robotic applications. The conceptual connections that can be established for a PCC soft continuum robot can be derived from the frameworks of rigid robot topologies. By employing the state-space representation of a corresponding rigid robot, it is possible to develop an enhanced model that accurately reflects the characteristics of a PCC soft continuum robot. In this context, let $\mu \in R^{n\times m}$ denote the augmented configuration of the PCC soft robot, where m represents the number of joints associated with each continuum segment.

The alignment of terminal points for each control curve segment with the respective reference points of the rigid robotic framework is guaranteed through the mapping process. From a kinematic point of view, any enhanced representation that meets the alignment criteria can be considered equivalent. This equivalence is essential for upholding the integrity of robotic motion, as it ensures that the kinematic relationships remain consistent across various configurations. An equivalent rigid robot, depicted in Fig. 4(c), is characterized by an RPPR configuration, where R denotes revolute joints and P indicates prismatic joints. To effectively model the mass distribution of the central chord segment, a point mass, denoted as W_i, is strategically placed at the midpoint of the main chord. The Denavit-Hartenberg (DH) parameters for this equivalent rigid body are detailed in Tab. I, where the parameters θ_{dh}, d, a, and α represent the conventional DH notation used for robotic kinematics.

TABLE I: DH parametrization table of equivalent rigid robot

Links	θ_{dh}	d	a	α	Mass
1	$\theta_w/2$	0	0	$\pi/2$	0
2	0	$l_i\frac{sin\frac{\theta_w}{2}}{\theta_w}$	0	0	W_i
3	0	$l_i\frac{sin\frac{\theta_w}{2}}{\theta_w}$	0	$-\pi/2$	0
4	$\theta_w/2$	0	0	0	0

The parameterized configuration of an individual segment, denoted as $\mu_i(\theta_w)$, consists of four elements and is derived through the application of Denavit-Hartenberg (DH) parametrization, as articulated in (2). This configuration serves as a crucial representation in the context of robotic kinematics, encapsulating the geometric and positional attributes of the segment in relation to its joint variables.

$$ \mu_i(\theta_w) = \begin{bmatrix} \frac{\theta_w}{2} & l_i\frac{sin\frac{\theta_w}{2}}{\theta_i} & l_i\frac{sin\frac{\theta_w}{2}}{\theta_i} & \frac{\theta_w}{2} \end{bmatrix}^T. \tag{2} $$

C. Dynamic Modelling of the Wrist

Dynamic modelling of the wrist was carried out using Euler-Lagrange formulation. Transpose of Jacobian with respect to

IEEE Transactions on Automation Science and Engineering (T-ASE) paper, presented at ICRA 2026, Vienna, Austria.

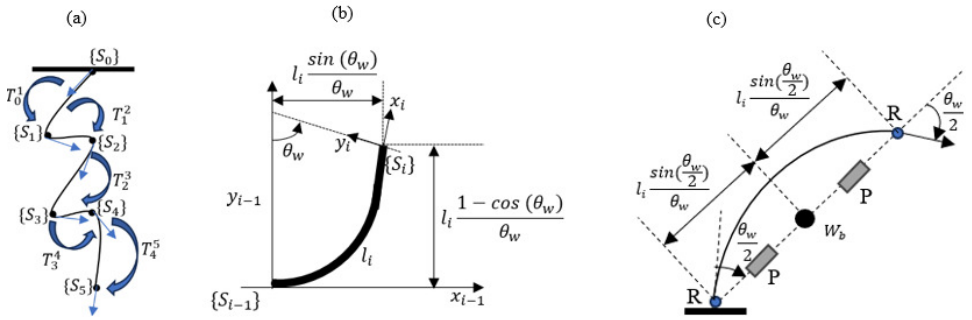

Fig. 4: Configuration. (a) Transformations. (b) Single segment. (c) RPPR.

θ_b, $\boldsymbol{J_\mu}(\theta_w) = \frac{\partial \mu}{\partial \theta_b}$ is given in (3)

$$\boldsymbol{J_\mu}(\theta_w) = \begin{bmatrix} \frac{1}{2} & l_w & l_w & \frac{1}{2} \end{bmatrix}^T. \tag{3}$$

where l_w is given in (4)

$$l_w = l_i \frac{\theta_w \ cos(\frac{\theta_w}{2}) - 2 \ sin(\frac{\theta_w}{2})}{2\theta_w^2} \tag{4}$$

(4) is used in dynamic modelling procedure for mapping the wrist section configuration to the 4-parameter configuration. The dynamic model of the wrist incorporating mapping Jacobian, $\boldsymbol{J_\mu}$ with respect to a generalised joint parameter, θ_w and their derivatives $(\dot{\theta}_w, \ddot{\theta}_w)$ is given in (5).

$$\begin{aligned} M(\theta_w)\ddot{\theta}_w + \Big(C(\theta_w, \dot{\theta}_w) + D\Big)\dot{\theta}_w + G(\theta_w) + K\theta_w \\ = \tau + \boldsymbol{J^T}(\theta_w)F_t \end{aligned} \tag{5}$$

where $M(\theta_w)$ is the $n \times n$ mapped inertia matrix with respect to the $4n \times 4n$ generalised inertia matrix $M_b(\theta_w)$, $C(\theta_w, \dot{\theta}_w)$ is the $n \times n$ mapped centrifugal with respect to the $4n \times 4n$ generalised centrifugal Coriolis matrix $C_b(\theta, \dot{\theta}_w)$, $G(\theta_w)$ is the $n \times 1$ mapped gravitational field with respect to the $4n \times 1$ gravitational field $G_b(\theta_w)$, D and K represent damping and stiffness values respectively. $M(\theta_w)$ is given in (6)

$$M(\theta_w) = \boldsymbol{J_\mu^T}(\theta_w) \ M_b(\mu(\theta_w)) \ \boldsymbol{J_\mu}(\theta_w). \tag{6}$$

$C(\theta_w, \dot{\theta}_w)$ is given in (7)

$$\begin{aligned} C(\theta_w, \dot{\theta}_w) = \boldsymbol{J_\mu^T}(\theta_w) \ M_b(\mu(\theta_w)) \ \boldsymbol{\dot{J}_\mu}(\theta_w, \dot{\theta}_w) + \\ \boldsymbol{J_(^T}\theta_w) \ D_b(\mu(\theta_w), \boldsymbol{J_\mu}(\theta_w)\dot{\theta}_w)\boldsymbol{J_\mu}(\theta_w). \end{aligned} \tag{7}$$

$G(\theta_w)$ is given in (8)

$$G(\theta_w) = \boldsymbol{J_\mu^T}(\theta_w) \ G_b(\mu(\theta_w)). \tag{8}$$

τ is the $n \times 1$ mapped actuation torque with respect to $4n \times 1$ mapped actuation torque, τ_b given in (9)

$$\tau = \boldsymbol{J_\mu^T}(\theta_w) \ \tau_b. \tag{9}$$

The relation between τ_b, $n \times 1$ tendon force (F_t), τ_b, and $n \times n_a$(n_a:number of actuators) actuation matrix (A_b) is given in (10)

$$\tau_b = A_b F_t. \tag{10}$$

Tendon force, F_t is obtained using the equation given in (11)

$$F_t = [\boldsymbol{J_\mu^T}(\theta_w)A_b]^{-1}\tau. \tag{11}$$

Jacobian, J is given in (12)

$$\boldsymbol{J} = \boldsymbol{J_b}(\theta_w) \ \boldsymbol{J_\mu}(\theta_w). \tag{12}$$

$\boldsymbol{J_b}$ maps external force to the joint torque values. In this work, we explicitly consider spring stiffness, K as an uncertain parameter due to potential degradation over time and variations in material properties. To address this uncertainty, our dynamic model incorporates spring stiffness as a variable rather than a fixed value, allowing it to fluctuate within a defined range. This approach ensures that the MRAC effectively adapts to changes in stiffness, maintaining the stability and performance of the prosthetic wrist. Instead of using a single stiffness value K, we defined it as a varying parameter as given in equation 13

$$K(t) = K_0 - \Delta K(t), \tag{13}$$

where K_0 is the nominal stiffness and t is the time. Change in stiffness, $\Delta K(t)$ is given in equation 14

$$K(t) = K_0(1 - e^{-\alpha t}), \tag{14}$$

where α is the degradation rate (determined experimentally). We measured the stiffness with response to tendon force during experimentation and calculated the degradation rate. Although stiffness is treated as a time-varying parameter, we must account for residual uncertainty arising from the nonlinear and potentially non-repeatable spring characteristics, which are not fully captured by the degradation model and are thus handled by the adaptive nature of the MRAC. Thus, in this work, we consider spring stiffness as an uncertain parameter. The dynamic model was employed in MRAC strategy to increase the accuracy of control action. In the following, since we only work with a single segment we will denote θ_w as the output bending angle of the wrist.

IV. Model Reference Adaptive Control Strategy

The MRAC approach employs a reference model to guide the control system's behavior, enabling dynamic adaptation to variations in system dynamics or external disturbances. In the case at hand, the wrist model presents a gravitational disturbance, due to the presence of the prosthetic hand at the top of the wrist, and a parametric stiffness uncertainty resulting from the natural degradation of the springs used in the soft wrist. By comparing the actual system output to the reference model, the adaptive control mechanism continuously adjusts the control gains, ensuring that the system's performance aligns closely

IEEE Transactions on Automation Science and Engineering (T-ASE) paper, presented at ICRA 2026, Vienna, Austria.

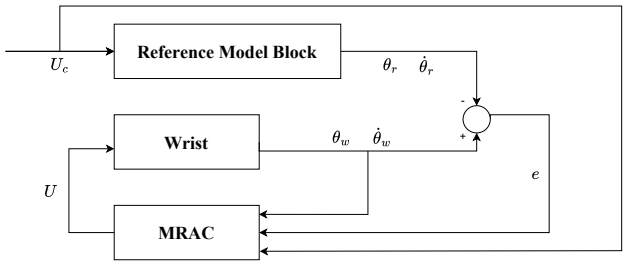

Fig. 5: General control scheme.

with the desired reference model. This approach is particularly advantageous in complex systems, where traditional control methods may struggle to maintain optimal performance due to changing or inaccurately modeled parameters. The MRAC scheme developed to control wrist motion is illustrated in Fig. 5.

In this control strategy, a reference signal U_c is given as the input into the reference model block (RMB). To define the reference model used, we start considering the following LTI system:

$$\dot{\boldsymbol{X}}(t) = \boldsymbol{A}\boldsymbol{x}(t) + \boldsymbol{B}U_c(t), \tag{15}$$

where the system state, $\boldsymbol{x}(t)$, is represented as:

$$\boldsymbol{x}(t) = \begin{bmatrix} x_1 \\ x_2 \end{bmatrix} = \begin{bmatrix} \theta_r \\ \dot{\theta}_r \end{bmatrix}. \tag{16}$$

Here, θ_r and $\dot{\theta}_r$ represent the position and velocity of the reference system, respectively. The coefficient matrices, $\boldsymbol{A}$ and $\boldsymbol{B}$, are defined as:

$$\boldsymbol{A} = \begin{bmatrix} 0 & 1 \\ -M^{-1}K & -M^{-1}(C+D) \end{bmatrix}. \tag{17}$$

$$\boldsymbol{B} = \begin{bmatrix} 0 \\ M^{-1} \end{bmatrix}. \tag{18}$$

The variables $M = M(\theta_d)$ and $C = C(\theta_d, \dot{\theta}_d)$, as computed in (6) and (7), define the matrices $\boldsymbol{A}$ and $\boldsymbol{B}$ that are time-invariant and configuration-independent. θ_d and $\dot{\theta}_d$ represent the desired bending angles input to the reference model. This results in an LTI system that approximates the internal dynamics of the wrist system, as described in equation (5). Notice that equation (15) does not yet describe the RMB; in this paper we compare the performance of the controller using two distinct reference models:

I) The first approach employs a reference model, the system in equation (15) controlled by a Proportional-Derivative (PD) controller, where the proportional K_P and derivative K_D gains are determined from the system's step response. The presence of the PD controller is necessary to make the reference model track the desired bending angle θ_d. The control input to the MRAC block $U_c = \theta_d$ is constant and equal to the desired bending angle;

II) The second approach uses the system described in equation (15) in open loop as the reference model. In this case, as the reference model in open loop is not guaranteed to track the desired bending angle θ_d, U_c, must actively regulate the reference model to track it. This requires a time-varying control input, $U_c = K_P(\theta_d - \theta_r) - K_D(\dot{\theta}_r)$, where K_P and K_D define the proportional and derivative control terms for the reference model, respectively. The elaborated scheme of the two control schemes is shown in Fig. 6. The key

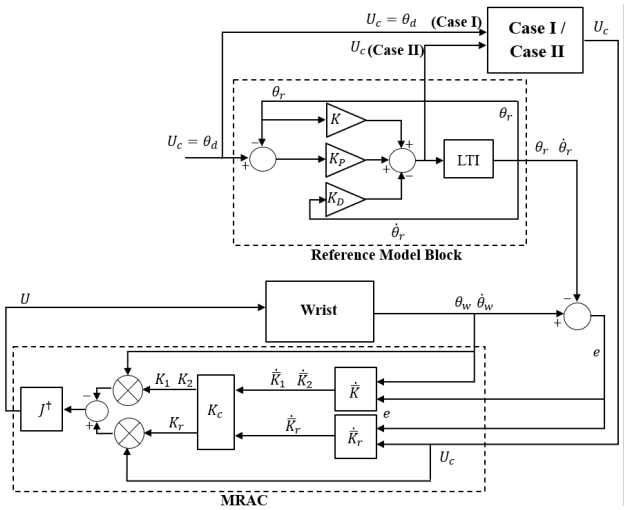

Fig. 6: Elaborated control scheme.

distinction between the two strategies lies in the MRAC input: in case I, U_c is constant and equal to θ_d as the PD controller is incorporated into the reference model. In case II, U_c is time-varying as the open-loop reference model described in equation (15) is employed, with the PD action embedded in the control law U_c. In this framework, the MRAC is interpreted as a means of forcing the nonlinear plant to follow the behavior of the chosen reference model. Consequently, the control design problem is shifted to ensuring that the reference model itself is capable of tracking the desired bending angle. Since the reference model is LTI, this objective can be readily achieved using a simple PD control strategy.

For both strategies, the output from the RMB is compared to wrist model's motion, and the error $\boldsymbol{E}$, is defined as:

$$\boldsymbol{E} = \begin{bmatrix} e \\ \dot{e} \end{bmatrix} = \begin{bmatrix} \theta_w - \theta_r \\ \dot{\theta}_w - \dot{\theta}_r \end{bmatrix}. \tag{19}$$

The MRAC block receives this error, along with the wrist output motions θ_w and $\dot{\theta}_w$, and U_c to generate a control law U, which is structured as:

$$U = K_r U_c - (K_1\theta_w + K_2\dot{\theta}_w) + G(\theta_w), \tag{20}$$

where the gains K_1, K_2, and K_r are time-varying and dependent on the error $\boldsymbol{E}$.

V. Stability Analysis

This section extends the results presented in [26] to include cases where the dynamic model controlled by the MRAC involves configuration-dependent and, thus, time-varying matrices. By considering the system described in (5) without

IEEE Transactions on Automation Science and Engineering (T-ASE) paper, presented at ICRA 2026, Vienna, Austria.

external forces, and substituting the control input from (20), we obtain the following system dynamics:

$$\ddot{\theta}_w = M(\theta_w)^{-1}K_r U_c - \Big(M(\theta_w)^{-1}K_2 + \Big(C(\theta_w,\dot{\theta}_w) + D\Big)\Big)\dot{\theta}_w + - \big(M(\theta_w)^{-1}K_1 + K\big)\theta_w. \quad (21)$$

Defining the state error e as in (19), and differentiating it twice, the resulting error dynamics are:

$$\ddot{e}+M^{-1}(C+D)\dot{e}+M^{-1}ke = \underbrace{\big(M(\theta_w)^{-1}K_r - M^{-1}\big)}_{\bar{K}_r} U_c + \\ + \underbrace{\Big(M^{-1}(C+D) - M(\theta_w)^{-1}K_2 - \Big(C(\theta_w,\dot{\theta}_w)+D\Big)\Big)}_{\bar{K}_2}\dot{\theta}_w + \\ + \underbrace{\big(M^{-1}k - M(\theta_w)^{-1}K_1 - K\big)}_{\bar{K}_1}\theta_w, \quad (22)$$

Here, we employ $\bar{K}_r$, $\bar{K}_1$ and $\bar{K}_2$ for compact notation. We can express in state-space form by introducing the vector $\boldsymbol{E} = \begin{bmatrix} e \\ \dot{e} \end{bmatrix}$ and defining the control term R as:

$$R = \bar{K}_r U_c + \bar{K}_2\dot{\theta}_w + \bar{K}_1\theta_w. \quad (23)$$

Thus, the error dynamics are expressed as:

$$\dot{\boldsymbol{E}} = \boldsymbol{A}\boldsymbol{E} + \boldsymbol{B}_e R, \quad (24)$$

where $\boldsymbol{A}$ is the same as in (17) and $\boldsymbol{B}_e = \begin{bmatrix} 0 \\ 1. \end{bmatrix}$. The term R represents a new control input in the dynamic system of the error $\boldsymbol{E}$. To analyze the stability properties of the closed-loop system in (24), we use a Lyapunov candidate function given by:

$$V(\boldsymbol{E},\bar{K}_r,\bar{K}_1,\bar{K}_2) = \frac{1}{2}\boldsymbol{E}^T\boldsymbol{P}\boldsymbol{E} + \frac{1}{2\gamma_r}\bar{K}_r^2 + \frac{1}{2\gamma_1}\bar{K}_1^2 + \frac{1}{2\gamma_2}\bar{K}_2^2, \quad (25)$$

Here, $\boldsymbol{P}$ is chosen such that $\boldsymbol{A}^T\boldsymbol{P} + \boldsymbol{P}\boldsymbol{A} = -\boldsymbol{Q}$ with $\boldsymbol{Q}$ being symmetric positive definite (SPD) matrix. Differentiating V and using (24) along with the definition of R in (23), we obtain:

$$\dot{V} = -\boldsymbol{E}^T Q\boldsymbol{E} + \bar{K}_r\left(\frac{\dot{\bar{K}}_r}{\gamma_r} + \boldsymbol{E}^T\boldsymbol{P}\boldsymbol{B}_e U_c\right) + \\ + \bar{K}_1\left(\frac{\dot{\bar{K}}_1}{\gamma_1} + \boldsymbol{E}^T\boldsymbol{P}\boldsymbol{B}_e\theta_w\right) + \bar{K}_2\left(\frac{\dot{\bar{K}}_2}{\gamma_2} + \boldsymbol{E}^T\boldsymbol{P}\boldsymbol{B}_e\dot{\theta}_w\right). \quad (26)$$

The gain dynamics are determined to force the non-negative terms in $\dot{V}$, V to zero as follows:

$$\begin{aligned} \dot{\bar{K}}_r &= -\gamma_r\boldsymbol{E}^T\boldsymbol{P}\boldsymbol{B}_e U_c. \\ \dot{\bar{K}}_1 &= -\gamma_1\boldsymbol{E}^T\boldsymbol{P}\boldsymbol{B}_e\theta_w. \\ \dot{\bar{K}}_2 &= -\gamma_2\boldsymbol{E}^T\boldsymbol{P}\boldsymbol{B}_e\dot{\theta}_w. \end{aligned} \quad (27)$$

Thus, we obtain the final result:

$$\dot{V} = -\boldsymbol{E}^T\boldsymbol{Q}\boldsymbol{E}. \quad (28)$$

Since $\dot{V}$ is negative semi-definite and V is positive definite, we can conclude that the systems described in equation (24) and equation (27) are stable (but not necessarily asymptotically), and their states are bounded. To prove asymptotic stability, we can use Barbalat's Lemma, but in this work, we rely on the results from the "New Theorem of Stability" proposed in [5]. According to this theorem, since V is bounded from below and $\dot{V}$ is negative semi-definite, the system's state, defined as $\boldsymbol{W} = \big[\boldsymbol{E}, \bar{K}_r, \bar{K}_1\bar{K}_2\big]^T$,will converge to a region $\boldsymbol{\Omega}$, where: $\boldsymbol{\Omega} = \Big\{\boldsymbol{W} \big| \lim_{t\to\infty}\dot{V}(\boldsymbol{W},t) \equiv \boldsymbol{0}\Big\}$. Therefore, with reference to (28), $\boldsymbol{X}$ has to converge so that $\boldsymbol{E} \equiv \boldsymbol{0}$ ($\boldsymbol{E}$ and its higher order derivatives converge to zero). Then, due to the presence of $\boldsymbol{E}$ in (27), we can conclude that $\bar{K}_r$, $\bar{K}_1$ and $\bar{K}_2$ also converge to constant fixed values.

In relation to (22), it can be inferred that, barring any singularities in $J_\mu(\theta_w)$, the gains K_r, K_1, and K_2 as indicated in (20) also stabilize at constant values, provided that $\boldsymbol{E}$ approaches zero and the reference model in (15) attains convergence. In order to implement the control law in (20), it is necessary to analyze the dynamics of the gains K_r, K_1, and K_2 in relation to $\bar{K}_r$, $\bar{K}_1$, and $\bar{K}_2$. This analysis should incorporate their dynamics as outlined in (27), while also taking into account that the wrist system matrices $M(\theta_w)$ and $C(\theta_w,\dot{\theta}_w)$ are configuration dependant. Therefore we have two solutions to compute the variable gains for the control input, namely:

1) Computing $\dot{\bar{K}}_r$, $\dot{\bar{K}}_1$ and $\dot{\bar{K}}_2$ from their definition given in (22) and substituting it in (27), we obtain $\dot{K}_r$, $\dot{K}_1$ and $\dot{K}_2$ as:
$$\begin{aligned} \dot{K}_r &= M(\theta_w)\Big(M(\theta_w)^{-1}\dot{M}(\theta_w)M(\theta_w)^{-1}K_r - \gamma_r\boldsymbol{E}^T\boldsymbol{P}\boldsymbol{B}_e U_c\Big). \\ \dot{K}_1 &= M(\theta_w)\Big(M(\theta_w)^{-1}\dot{M}(\theta_w)M(\theta_w)^{-1}K_1 + \gamma_1\boldsymbol{E}^T\boldsymbol{P}\boldsymbol{B}_e\theta_w\Big). \\ \dot{K}_2 &= M(\theta_w)\Big(M(\theta_w)^{-1}\dot{M}(\theta_w)M(\theta_w)^{-1}K_2 - \dot{C}(\theta_w,\dot{\theta}_w) + \gamma_2\boldsymbol{E}^T\boldsymbol{P}\boldsymbol{B}_e\dot{\theta}_w\Big). \end{aligned} \quad (29)$$
Finally, we can perform the integration of (29) to obtain the values of K_r, K_1, and K_2.
2) Integrating (27) to obtain $\bar{K}_r$, $\bar{K}_1$ and $\bar{K}_2$, and then using (22) to retrieve K_r, K_1 and K_2;

In our implementation we opted for the second solution, to avoid computational time to calculate $\dot{M}(\theta_w)$ and $\dot{C}(\theta_w,\dot{\theta}_w)$.

VI. Result and Discussion

This study demonstrated the modeling and controller design of a wrist part designed to support the payload and dexterous movements of an existing prosthetic hand. A comparison was made between the proposed MRAC scheme and other controllers developed for the wrist section in the coming sections. This section also includes simulation studies and experimental validations of the MRAC to evaluate effectiveness of the controller in real tasks.

A. Simulation Study

The MRAC was implemented and tested in the Simulink environment, which is a component of MATLAB, running on an Intel Core i7 processor and 16 GB of RAM. The wrist motions without carrying prosthetic hand in ulnar, radial, flexion, and extension directions are shown in Fig. 7. The wrist was simulated to bend from its initial position to a desired angle $\theta_d = 30^o$ in ulnar, radial, flexion, and extension directions relative to disc 5, attached to the hand as shown in Fig. 8.

IEEE Transactions on Automation Science and Engineering (T-ASE) paper, presented at ICRA 2026, Vienna, Austria.

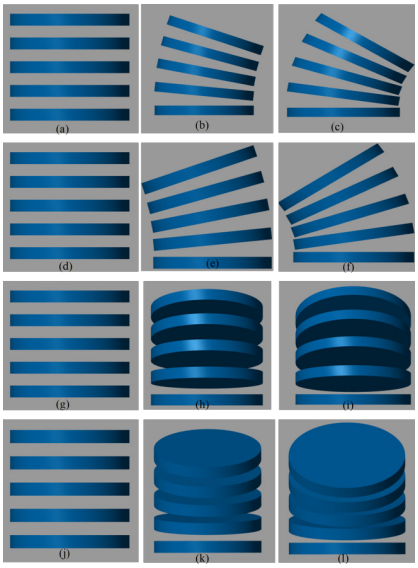

Fig. 7: Motion of wrist in all directions (a)-(c)Ulnar (d)-(f)Radial (g)-(i)Flexion(j)-(l)Extension

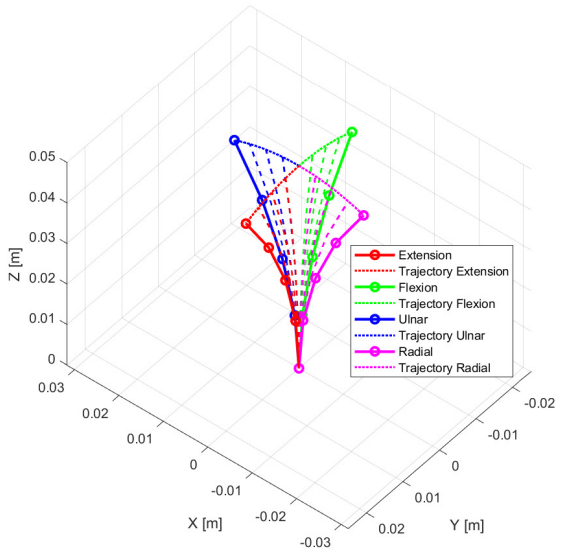

Fig. 8: Trajectory of wrist in all directions.

The proposed MRAC regulated wrist movements, as detailed in Section IV, utilizing two strategies: controlled reference model (strategy I) and open-loop reference model (strategy II). For the simulations, the gains for the PD controller were set as $K_P = 10$ and $K_D = 5$ for both strategies. The wrist's damping and nominal stiffness were determined as 0.615 Nm and 0.105 Nms, respectively. The values of γ_1, γ_2, and γ_r were obtained as 2, 5, and 10 respectively. Initially, we conducted simulations to analyze the motion of the wrist sections independently, without including the hand segment. Because the structure of the wrist is symmetric, meaning its physical and mechanical properties are mirrored across an axis and the dynamic response characteristics remained consistent across different simulations. Specifically, the system demonstrated uniformity in terms of gain convergence, settling time, steady-state error, and general behavior. This indicates that the

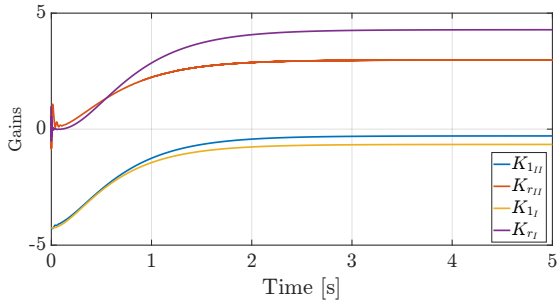

Fig. 9: Evolution of gains K_1 and K_r.

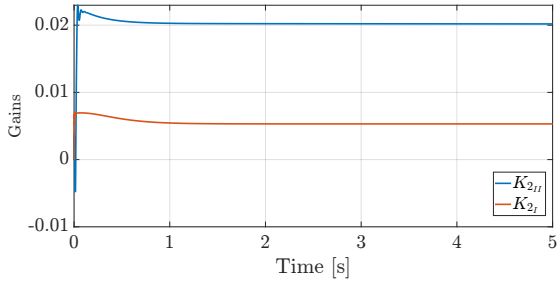

Fig. 10: Evolution of gain K_2.

system's performance is predictable and stable regardless of orientation or side. The variations in adaptive gains during the simulation are shown in Figs. 9 and 10, confirming that the adaptive gains converged to fixed values as stated in the stability analysis in Section V. In Figs. 9 and 10, it is evident that the gains converged to a fixed value around 2 s. The key difference between the two strategies was that strategy I (using the controlled reference model) resulted in lower fixed values for K_1 and K_2, and a higher regime value for K_r, while strategy II (using the open-loop system) achieved higher values for these gains. The errors between the desired and actual bending angles are shown in Fig. 11, where the RMSE values for strategies I and II were 1.2×10^{-3} Rad and 1.4×10^{-3} Rad, respectively. The settling times for strategies I and II were measured as 2.8 s and 3.2 s, with steady-state errors of 1.3×10^{-3} Rad and 1.6×10^{-3} Rad, respectively. All values were within acceptable tolerance limits, with strategy I performing slightly better as evident from steady state error and settling time values. Furthermore, the variations in the adaptive gains $\bar{K}_r$, $\bar{K}_1$ and $\bar{K}_2$ for both control laws are shown

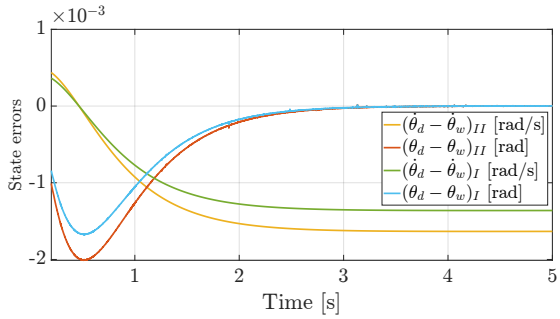

Fig. 11: Steady state error during simulation.

IEEE Transactions on Automation Science and Engineering (T-ASE) paper, presented at ICRA 2026, Vienna, Austria.

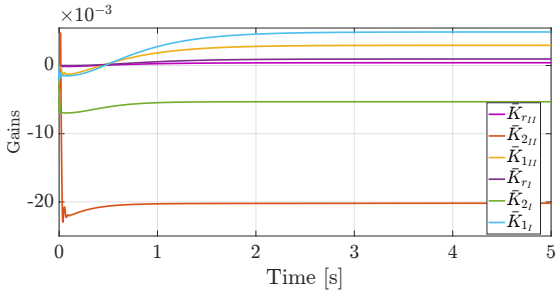

Fig. 12: Evolution of gains $\bar{K}_r$, $\bar{K}_1$ and $\bar{K}_2$.

in Fig. 12. These gains converged in a time period within 2.5 s. As discussed in Section V, the system described in equation (24) is proved to be stable. This implied that the term B_eR must asymptotically tend toward zero. Consequently, given the definition of R in (23), the values of $\bar{K}_1$ and $\bar{K}_2$, weighting the error e and its derivative $\dot{e}$, respectively, converged to non-zero values, as e and $\dot{e}$ tend towards 0. Conversely, $\bar{K}_r$, associated with the control input U_c, converged to a value near zero as U_c approached its non-zero steady-state value. The findings substantiated the efficacy of the MRAC in attaining consistent performance stability. Due to the symmetrical structure of the wrist section, identical results were obtained in all directions. To investigate the effects of incorporating a hand, additional simulation studies were conducted.

In order to analyse the performance of the controllers to an external force when the wrist section was carrying the prosthetic hand, a constant force of $1N$ is applied to the mid section of prosthetic hand perpendicular to the direction of motion as shown in Fig. 13 and the responses were obtained as shown in Fig. 14. Since the force acts in a time period of

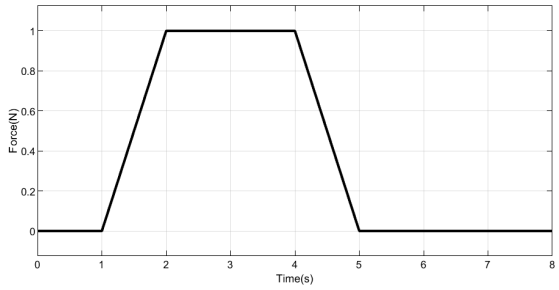

Fig. 13: Constant force applied to prosthetic hand

1 second to 5 s, the gains K_1, K_2, K_3, and the error values fluctuate in this time period. However, the gains and error converged as shown in Fig. 14 around 6.2 s (average of two methods). An impulsive force of $1\ N$ is applied to the wrist section for a time duration of $0.5\ s$ starting from $1\ s$ as shown in Fig. 15. K_1, K_2, K_3, and the error values of I^{st} and II^{nd} methods were obtained as shown in Fig. 16. During the time interval between 1 and 1.5 s, the system is subjected to an external force, which results in fluctuations in the controller gains K_1, K_2, and K_3, as well as the corresponding error values. This dynamic response is expected, as the system adjusts to the applied load. Despite these initial variations, both the gains and errors of two methods gradually converge, achieving stability at approximately 5.275 s (average of two methods).

To investigate the impact of varying spring stiffness on the system's behavior, a simulation study was conducted by adjusting the stiffness values within a ±20% range relative to the nominal value. This variation is visually represented in Fig. 17 and 18. Fig.17 illustrates the system's response to two methods when the stiffness parameters—namely K_1, K_2, and K_r were decreased by 20%. The graph includes the corresponding error values recorded during the motion of the wrist section, which was simulated while carrying the prosthetic hand. In contrast, Fig. 18 presents results from increasing the same stiffness values by 20%, again monitoring the same system parameters during wrist motion. Throughout the simulation, the system exhibited noticeable variations in dynamic behavior due to these stiffness changes. Initial fluctuations in performance were observed; however, the system eventually reached a stable state. The responses converged at approximately 1.66 s for both of the cases for two controllers, demonstrating the system's ability to adapt to stiffness modifications while maintaining steady performance over time. Additionally, a stability test was performed by increasing the load on the hand by 50% to assess the controllers' robustness under higher external forces. The resulting behavior remained consistent with previous findings, the system maintained stability, and converged around 1.35 s as shown in Fig. 19.

Simulation-based Evaluation of MRAC Performance

To comprehensively evaluate the dynamic behavior of the wrist section under various conditions, the results obtained during simulation studies were compared. The analysis encompassed wrist motions in four primary directions: ulnar deviation, radial deviation, flexion, and extension. Each directional motion was examined using two distinct control methodologies, resulting in two simulation outcomes per direction. The simulation scenarios were designed to explore the system's performance under varying external conditions. Specifically, we investigated: (i) varying load magnitudes, (ii) modifications in spring stiffness within ±20% of the nominal values, (iii) application of constant external forces, and (iv) response to impulsive force inputs. For each simulation run, the system's performance was quantitatively assessed by recording three key metrics: root mean square error (RMSE), settling time, and steady-state error as shown in Table II.

The simulation results presented in Table II provide a comprehensive assessment of the Model Reference Adaptive Controller (MRAC) under various external force conditions, stiffness variations, and load disturbances. Each scenario was evaluated using two methodologies: Method I, representing closed-loop performance, and Method II, reflecting open-loop control behavior. Under constant force conditions, MRAC maintained exceptional precision. Method I yielded an impressively low RMSE of 1.0×10^{-4} Rad, with a steady-state error of just 5.0×10^{-5} Rad. Method II demonstrated a slightly higher RMSE of 2.8×10^{-3} Rad and steady-state error of 1.3×10^{-3} Rad, with corresponding settling times of 6.1 s and 6.3 s, respectively. These results highlight the controller's consistency and resilience under sustained external loading.

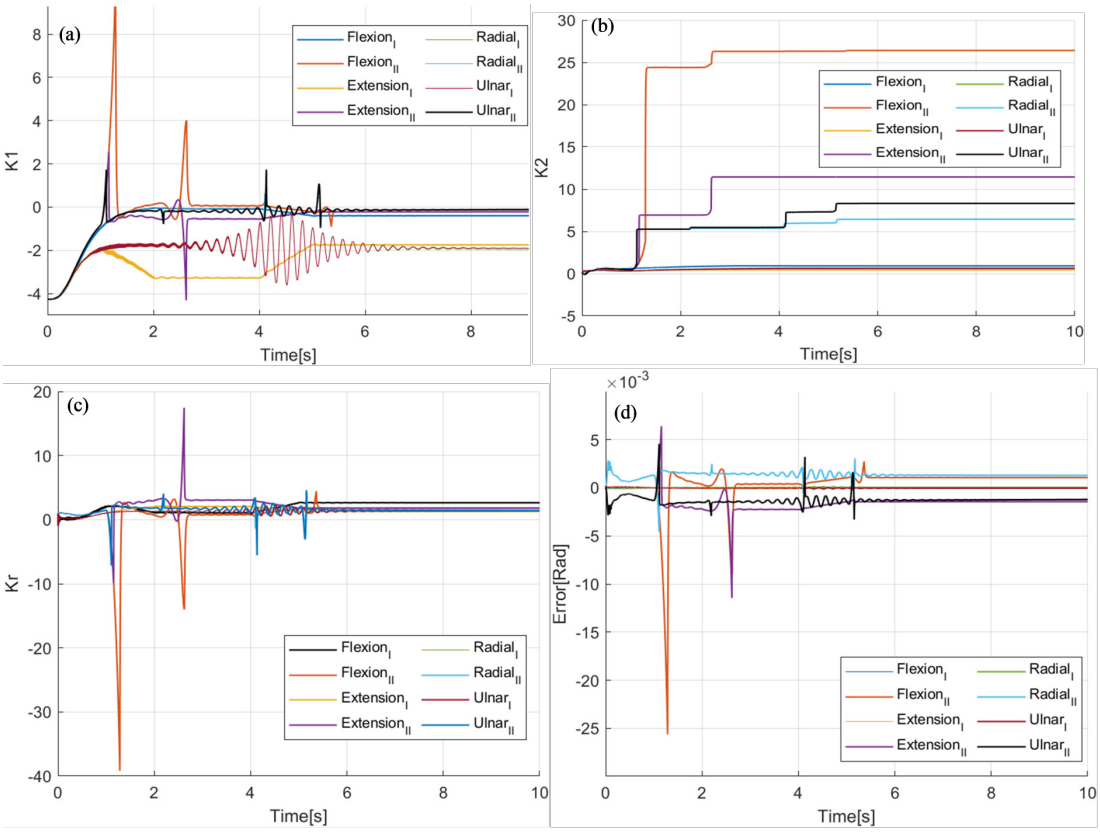

Fig. 14: Simulation results during an application of constant force (a)K_1 (b)K_2 (c)K_r (d)Error

TABLE II: Comparison study

Simulation study	RMSE(Rad)	Settling time(s)	Steady state error(Rad)
Constant force-I	1.00×10^{-4}	6.10	5.00×10^{-5}
Constant force-II	2.80×10^{-3}	6.30	1.30×10^{-3}
Impulse force-I	1.10×10^{-3}	5.20	9.00×10^{-4}
Impulse force-II	1.30×10^{-3}	5.35	1.30×10^{-3}
-20% stiffness-I	8.00×10^{-4}	1.60	5.00×10^{-4}
-20% stiffness-II	1.20×10^{-3}	1.70	1.10×10^{-3}
+20% stiffness-I	1.00×10^{-3}	1.62	2.10×10^{-4}
+20% stiffness-II	1.20×10^{-3}	1.75	1.20×10^{-3}
+50% load-I	9.00×10^{-4}	1.30	3.00×10^{-4}
+50% load-II	2.81×10^{-3}	1.40	2.70×10^{-3}

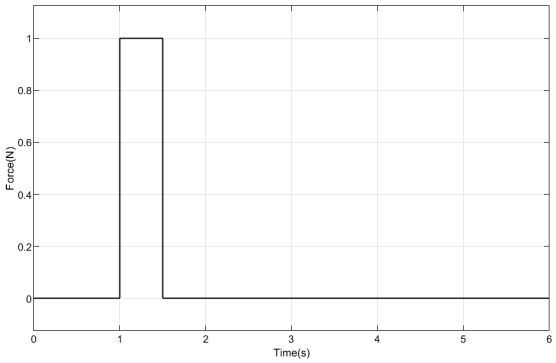

Fig. 15: Impulsive force applied to prosthetic hand

When subjected to impulsive force disturbances, MRAC continued to perform reliably. The RMSE values were 1.1×10^{-3} Rad and 1.3×10^{-3} Rad for Methods I and II, respectively. Both approaches showed settling times below 5.5 s and steady-state errors under 1.3×10^{-3} Rad, indicating the controller's strong capability to suppress transient perturbations effectively. In the context of decreased stiffness by 20%, MRAC achieved rapid responses, with settling times of 1.6 s and 1.7 s for Methods I and II. The closed-loop configuration maintained a lower RMSE of 8.0×10^{-4} and a steady-state error of 5.0×10^{-4} Rad. Conversely, increasing stiffness by 20% resulted in RMSEs of 1.0×10^{-3} Rad (Method I) and 1.2×10^{-3} Rad (Method II), with both methods maintaining settling times under 2 s and acceptable steady-state errors. These outcomes suggest strong adaptive capability to changes in system rigidity. Under a 50% increase in load, Method I achieved an RMSE of 9.0×10^{-4} Rad, settling time of 1.3 s, and steady-state error of 3.0×10^{-4} Rad. Method II showed a slightly faster response (1.40 s), though with

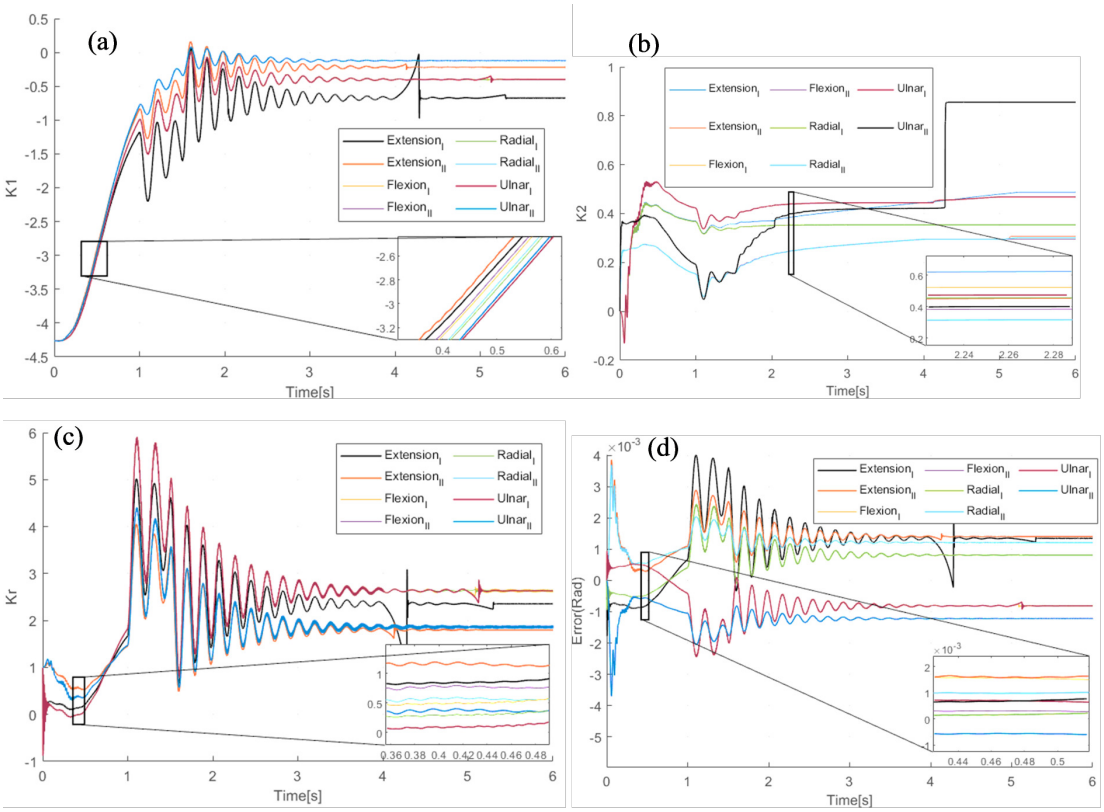

Fig. 16: Simulation results during an application of impulsive force (a)K_1 (b)K_2 (c)K_r (d)Error

higher error values—RMSE of 2.8×10^{-3} Rad and steady-state error of 2.7×10^{-3} Rad. In summary, the MRAC framework demonstrated robust adaptability and stability across diverse dynamic scenarios. Method I generally offered finer precision, while Method II excelled in responsiveness and control under closed-loop operation, confirming the controller's suitability for real-time prosthetic applications with uncertain dynamics.

B. Experimental Validation of MRAC

Experimental validations were carried out using a fabricated model of the wrist (shown in Fig. 1(b)) to analyse performance of the proposed controller. The presence of an ArUco marker affixed to the wrist allowed for precise tracking of the movements of disc 5 throughout the experimental procedures. Desired motions were fed into the controller as input, which subsequently generated the desired force outputs. To ensure the reliability and repeatability of the experimental results, each target trajectory was executed (5 times) under identical conditions. These outputs were then transformed into motor torque values, which were further converted into PWM signals. These signals were sent to an Arduino Mega 2560, which was interfaced with two stepper motors via a microstep driver (DM542). To enhance the efficiency of the operation, an Arduino module was incorporated with Simulink to facilitate the transmission of the computed input signals, while a ROS module was utilized to communicate the data from the ArUco markers back into the Simulink framework.

To provide concrete validation, we have included real-time computational performance metrics measured on the Arduino Mega 2560. Specifically, we report a control cycle time of 15 ms, a processing latency of 5 ms, and a CPU utilization of 35% during execution. The PWM update frequency has now been explicitly documented at 1 kHz, illustrating how the controller maintains real-time responsiveness. This ensured that motor control remained stable and precise under varying load conditions. Our experiments showcased an execution time of 8 ms per cycle, ensuring efficient performance. Additionally, preliminary results from ROS-based implementations indicated a latency of 12 ms, demonstrating the feasibility of real-time deployment.

The configuration of the experimental setup, which encompasses all relevant interfaces, is illustrated in the accompanying Fig. 20. Initially, the wrist motions without carrying hand were recorded in the ulnar, radial, flexion, and extension directions. The experimental setup revealed that the RMSE for the bending angles, settling time, and steady-state error were obtained as 0.057 Rad, 3.5 s, and 0.013 Rad respectively. The variations in the adaptive gains and the errors associated with the hand's motion are displayed in Figs. 21 - 23, where the convergences of the gains are clearly visible. K_1 and K_r gains converged around 5 s, whereas K_2 converged around 3 s. The time taken for converging was higher as compared to simulation study results, since real time experimentations were carried out on the wrist carrying a prosthetic hand. The weight of the prosthetic hand was acting as an unknown gravitational

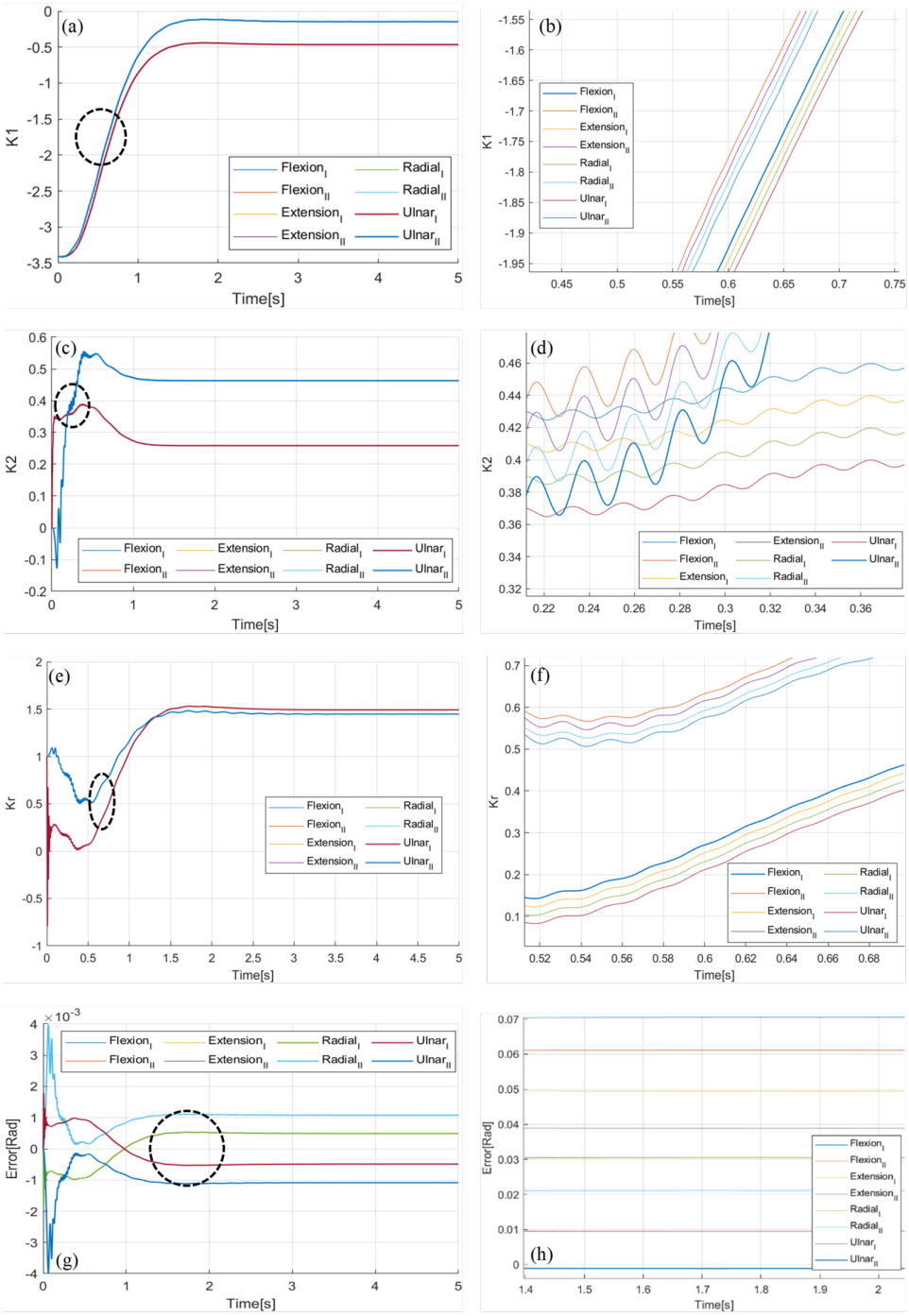

Fig. 17: Simulation results considering 20% less stiffness (a)K_1 (b)Enlarged view of K_1 (c)K_2 (d)Enlarged view of K_2 (e)K_r (f)Enlarged view of K_r (g)Error (h)Enlarged view of error

disturbance throughout the experimentation process. Additionally, the wrist stiffness K and damping D were uncertain, as continuous use led to wrist degradation, causing deviations of these parameters from their nominal values. However, the convergence of the gains showcased the effectiveness of the controller to adapt to unknown external disturbances and parametric uncertainties. Comparing the values of settling time and steady state error from the experimental phase with the simulation study, it was observed that the values were notably higher in the experimental trials. This discrepancy was primarily attributed to the reduced stiffness of the springs in the wrist segment, as well as the increased and unmodeled mass of the upper hand structure. Despite this, the wrist was able to successfully support the payload, maintaining stability throughout the motions.

After evaluating the motions of wrist section, we integrated the prosthetic hand to the wrist section to analyse the performance of the proposed controller in presence of prosthetic hand load. The motions of the wrist section along with prosthetic hand implemented using two methods in ulnar,

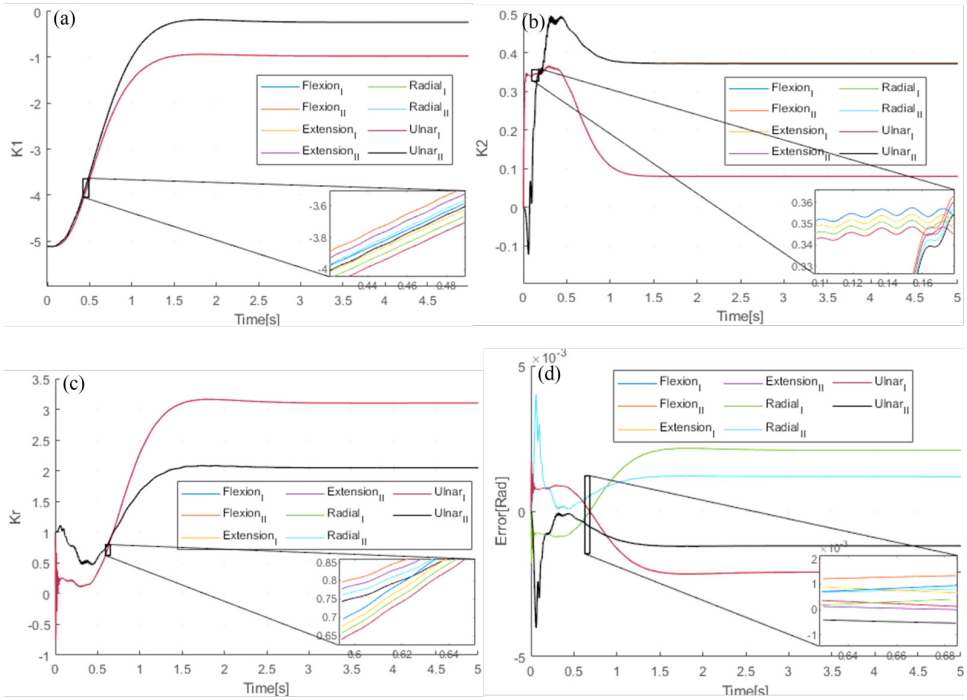

Fig. 18: Simulation results considering 20% more stiffness (a)K_1 (b)K_2 (c)K_r (d)Error

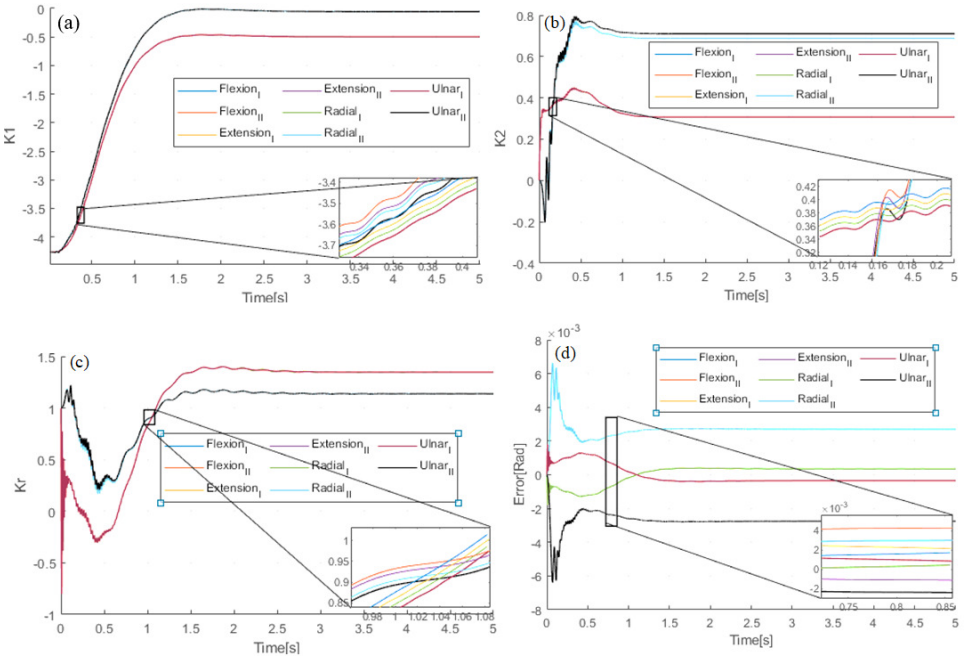

Fig. 19: Simulation results considering 50% more load (a)K_1 (b)K_2 (c)K_r (d)Error

radial, flexion, and extension directions are shown in Figs. 24 and 25. K_1, K_2, K_r gains and errors during experimentations are given in Figs. 26 - 29 respectively. Gains and errors converged around 2.7 s showcased the effectiveness of the controller in maintaining the motions along with the load of prosthetic hand. RMSE, settling time and steady state errors obtained during I^{st} method were determined as 0.052 Rad, 4.01 s, and 0.021 Rad respectively . However, RMSE, settling time and steady state errors obtained during II^{nd} method were showcasing higher values and determined as 0.060 Rad, 4.68 s, and 0.032 Rad respectively.

To validate the adaptiveness of the controller under external unknown forces, an external disturbance was manually applied using a human hand while the wrist without carrying hand was performing motions, as shown in Figs. 30- 33. Variations in K_1, K_2, and K_r are shown in Figs. 34 - 36 respectively. Although there are some initial fluctuations due to the application of force at the 0.5 -1. second mark, the gains are shown to

IEEE Transactions on Automation Science and Engineering (T-ASE) paper, presented at ICRA 2026, Vienna, Austria.

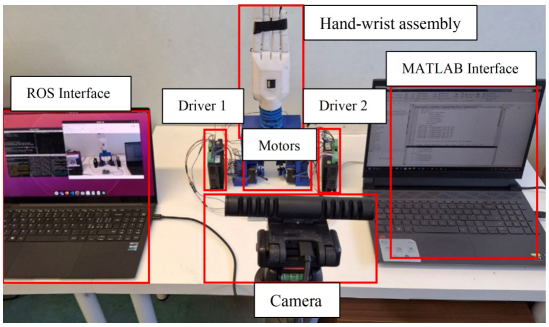

Fig. 20: Experimentation setup with all components

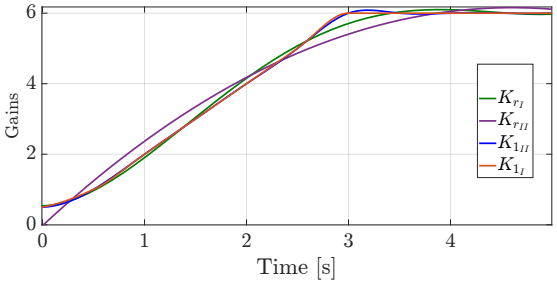

Fig. 21: Evolution of gains K_1 and K_r.

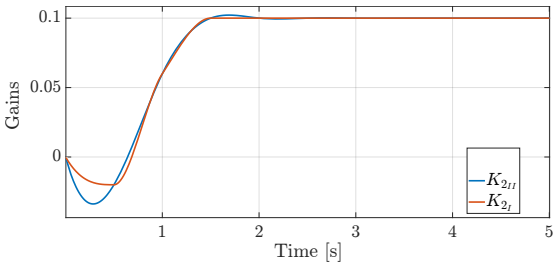

Fig. 22: Evolution of gain K_2.

be converging before 3 s. The resulting motion errors during the disturbance are presented in Fig. 37. An average RMSE values of 0.047 Rad and 0.061 Rad were recorded for I^{st} and II^{nd} methods respectively during this period. These results demonstrate the controller's capability to adapt effectively, as evidenced by the significantly reduced RMSE. Although fluctuations are observed during the application of external force around the 2-second mark, the gains show a clear trend of convergence. Additionally, the error values gradually reduce and stabilize, with convergence observed around 3 s. Settling time for methods I and II were obtained around 3s. Similiarly, steady state errors were obtained as 0.049 rad and 0.0399 Rad for methods I and II respectively.

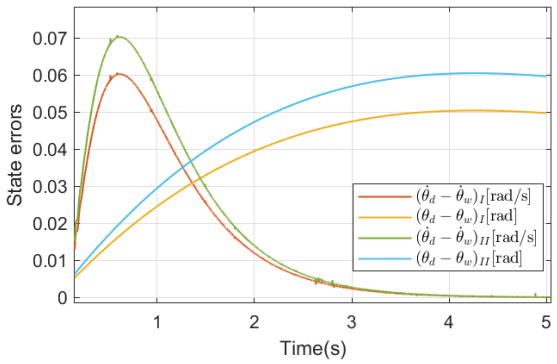

Fig. 23: Steady state error during experimentation.

C. Comparative Study With Other Controllers

The performance of the MRAC was compared with other controllers developed for the wrist section. RMSE, settling time and steady state error were compared to determine a better controller for the desired tasks as given in Tab. III. Comparison of the proposed MRAC with an L-MRAC [27], a Geometric Variable Strain based Controller (GVSC) [28], and a Conventional PID based controller [28] developed for the wrist to control motion in all directions are given in Tab. III.

The evaluation considers three key performance metrics—Root Mean Square Error (RMSE), Settling Time, and Steady-State Error—across four distinct wrist motions: ulnar, radial, flexion, and extension.

In terms of RMSE, the MRAC demonstrated consistent accuracy, with values ranging from 1.28×10^{-3} (radial) to 1.47×10^{-3} (flexion). L-MRAC yielded slightly lower errors across all motions, for example 5.78×10^{-4} in flexion and 6.14×10^{-4} in ulnar motion. This precision indicated L-MRAC's strength in nominal, well-modeled environments. However, MRAC achieved a comparable level of performance while offering improved adaptability to uncertainty and external disturbances. GVSC and PID controllers recorded significantly higher RMSEs in every motion, with PID showing peak errors up to 0.0055. The settling time analysis revealed that MRAC is responsive and stable across all axes, stabilizing between 2.70 s (ulnar) and 3.20 s (radial). These values were generally better than PID, which exhibits sluggish behavior with settling times as high as 5.74 s. Although L-MRAC showed competitive timings—for instance, 2.95 s in extension, its performance varies more widely. GVSC showed moderate settling performance but lacks the adaptiveness necessary for uncertain environments.

Steady-state error performance again underscores the robustness of MRAC, which maintained values below 2×10^{-3} for all motions. L-MRAC delivered comparably low final errors, such as 10.12×10^{-4} in flexion and 13.12×10^{-4} in ulnar movement. In contrast, GVSC showed higher residual

IEEE Transactions on Automation Science and Engineering (T-ASE) paper, presented at ICRA 2026, Vienna, Austria.

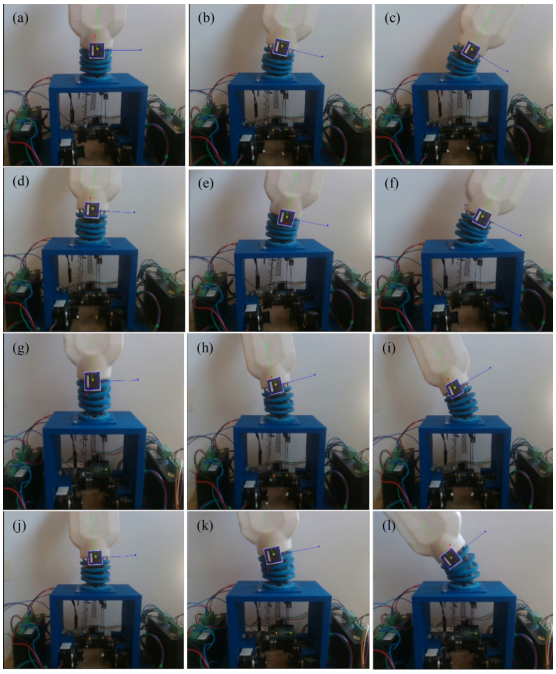

Fig. 24: Motions of wrists section carrying hand(a)-(c)Ulnar$_I$ (d)-(f)Ulnar$_{II}$ (g)-(i)Radial$_I$ (j)-(k)Radial$_{II}$

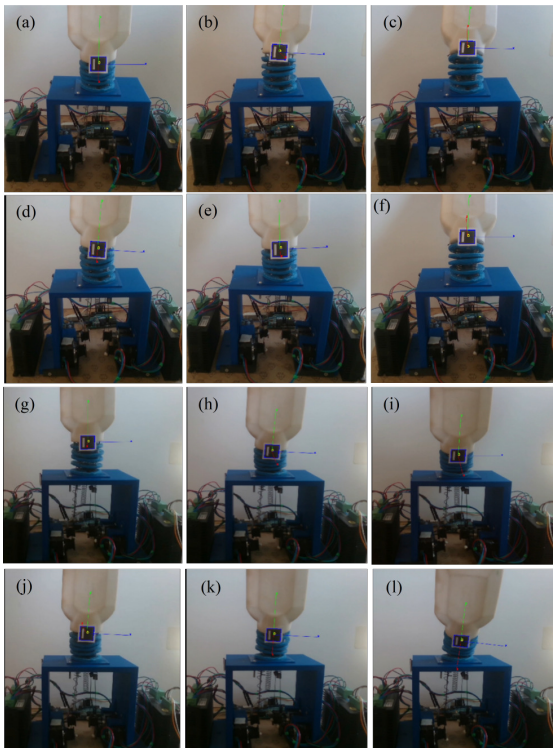

Fig. 25: Motions of wrists section carrying hand(a)-(c)Flexion$_I$ (d)-(f)Flexion$_{II}$ (g)-(i)Extension$_I$ (j)-(k)Extension$_{II}$

drift, reaching 0.019 in extension, while PID suffers the most, with steady-state errors exceeding 1.2 in all cases. In summary, while L-MRAC achieved slightly lower RMSE and steady-state errors in ideal conditions, MRAC provided a more balanced and resilient performance across all metrics, especially in the face of dynamic disturbances and uncertain parameters. This made MRAC a highly promising approach for real-time prosthetic control, where adaptability and precision are paramount. The RMSE, settling time and steady state error obtained using MRAC are found to be less as evident from Table. III. Hence, the proposed MRAC scheme was found to be more efficient in controlling the given task with fewer errors using lower computational efforts.

Similarly, when experimental results were compared, the

IEEE Transactions on Automation Science and Engineering (T-ASE) paper, presented at ICRA 2026, Vienna, Austria.

TABLE III: Comparison study of simulation results

Parameters	MRAC	L-MRAC [27]	GVSC [28]	PID [28]
RMSE:				
Ulnar	1.35×10^{-3}	6.14×10^{-4}	4.20×10^{-3}	5.20×10^{-3}
Radial	1.28×10^{-3}	5.99×10^{-4}	5.20×10^{-3}	5.50×10^{-3}
Flexion	1.47×10^{-3}	5.78×10^{-4}	2.70×10^{-3}	3.30×10^{-3}
Extension	1.29×10^{-3}	6.30×10^{-4}	4.20×10^{-3}	4.60×10^{-3}
Settling time:				
Ulnar	2.70	3.05	3.18	5.74
Radial	3.20	3.24	3.41	5.33
Flexion	3.07	3.40	2.81	4.24
Extension	3.18	3.27	2.46	4.91
Steady state error:				
Ulnar	1.05×10^{-3}	1.31×10^{-3}	1.40×10^{-2}	2.11×10^{-2}
Radial	1.01×10^{-3}	1.61×10^{-3}	1.50×10^{-2}	2.26×10^{-2}
Flexion	1.75×10^{-3}	1.01×10^{-3}	1.10×10^{-2}	2.07×10^{-2}
Extension	1.95×10^{-3}	1.71×10^{-3}	1.90×10^{-2}	2.04×10^{-2}

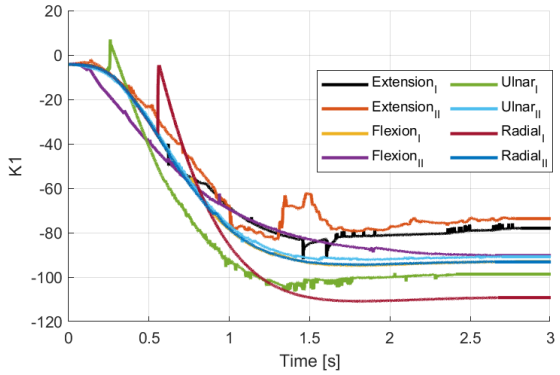

Fig. 26: K_1 gains during experimentation including prosthetic hand

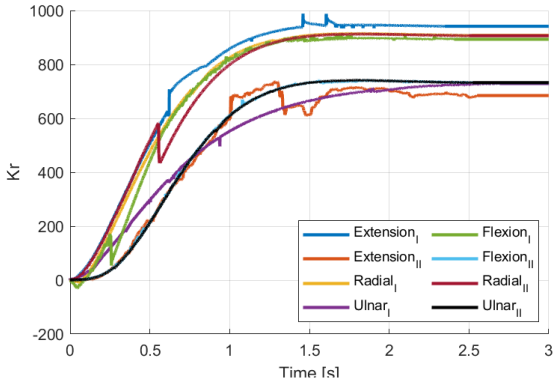

Fig. 28: K_r gains during experimentation including prosthetic hand

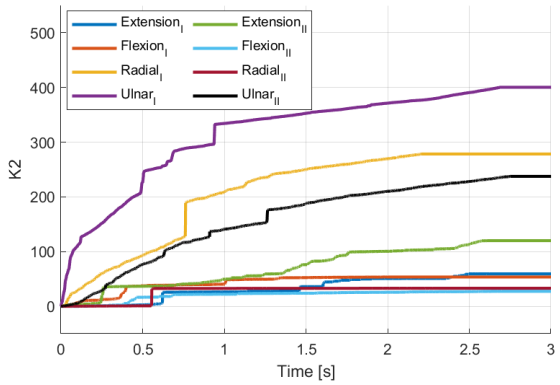

Fig. 27: K_2 gains during experimentation including prosthetic hand

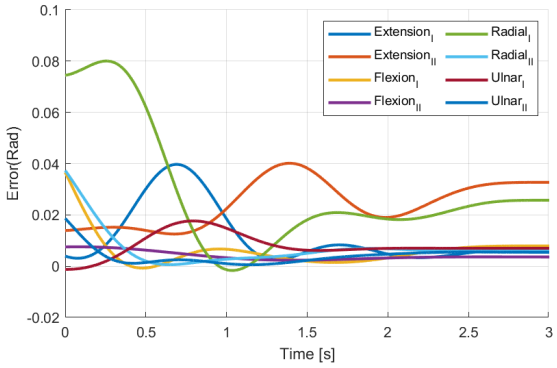

Fig. 29: Error obtained during experimentation including prosthetic hand

proposed MRAC showcased better performance compared to GVSC and PID in terms of RMSE, settling time, and steady-state error. L-MRAC exhibited lower RMSE and steady-state error values; however, its settling time was comparatively higher. This enhanced precision in L-MRAC can be attributed to the fact that it was developed using the MRAC control framework as a baseline, with its parameters optimally tuned based on extensive simulation and system characterization. As a result, L-MRAC inherently benefited from the foundational strengths of MRAC, which contributes to its favorable outcomes in both simulation and experimental trials.

The performance of the proposed MRAC has been evaluated and compared with various controllers designed for soft robots, based on error obtained from both simulations and experimental studies, as presented in IV. The errors exhibited by MRAC implemented on various systems are in the range of 10^{-4} to 10^{1}. The average value of errors exhibited by the proposed MRAC were in the range of 10^{-3} and in the tolerance range. Additionally, the errors obtained across various soft robotic control using PCC modelling studies highlight the differences between simulation-based assessments and experimental validations. In the study on dynamic task space control

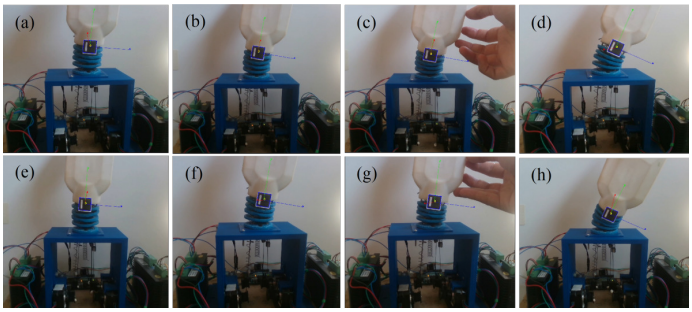

Fig. 30: Motions of wrists section carrying hand (a) -(b)Motions in ulnar direction-I (c)Application of external force-I (d)Recovery from force-I (e)-(f)Motions in ulnar direction-II (g)Application of external force-II (h)Recovery from force-II

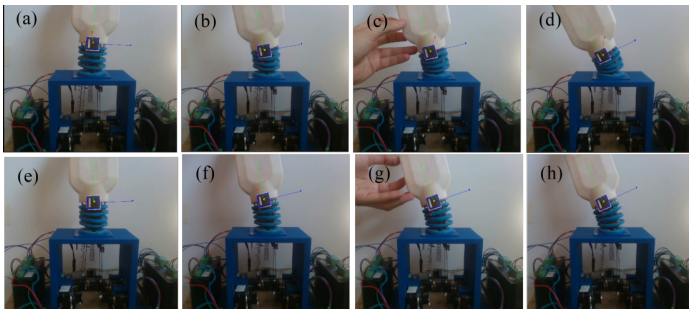

Fig. 31: Motions of wrists section carrying hand (a) -(b)Motions in radial direction-I (c)Application of external force-I (d)Recovery from force-I (e)-(f)Motions in radial direction-II (g)Application of external force-II (h)Recovery from force-II

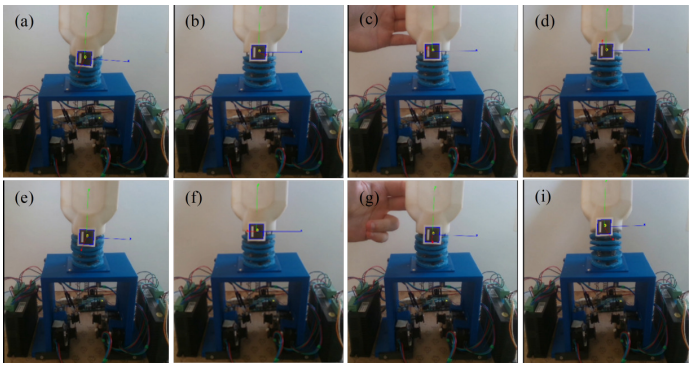

Fig. 32: Motions of wrists section carrying hand (a) -(b)Motions in flexion direction-I (c)Application of external force-I (d)Recovery from force-I (e)-(f)Motions in flexion direction-II (g)Application of external force-II (h)Recovery from force-II

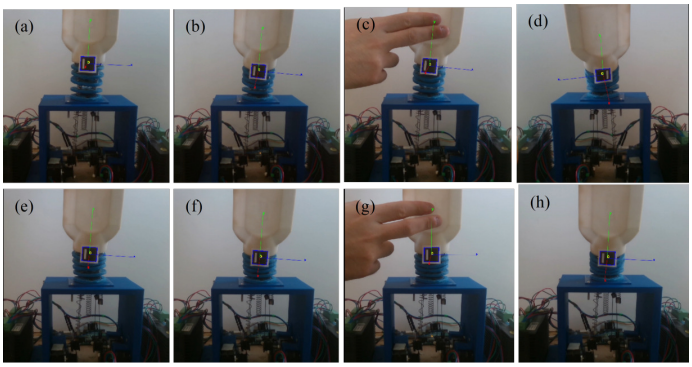

Fig. 33: Motions of wrists section carrying hand (a) -(b)Motions in extension direction-I (c)Application of external force-I (d)Recovery from force-I (e)-(f)Motions in extension direction-II (g)Application of external force-II (h)Recovery from force-II

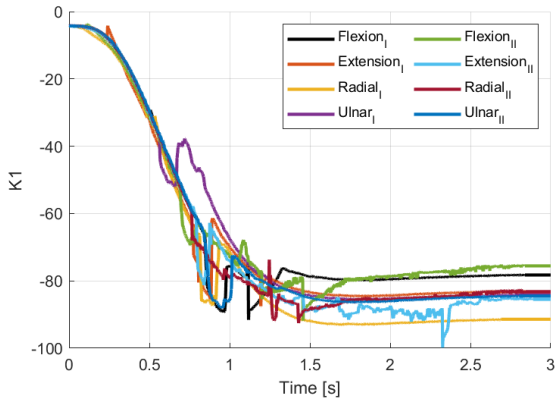

Fig. 34: K_1 gains obtained during experimentation in presence of external disturbances

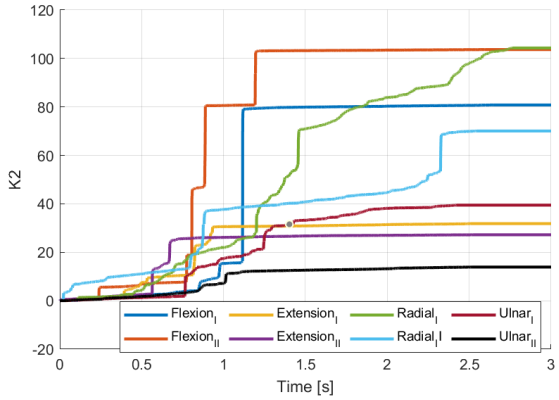

Fig. 35: K_2 gains obtained during experimentation in presence of external disturbances

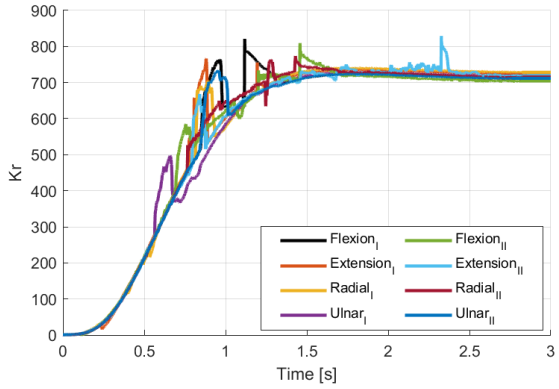

Fig. 36: K_r gains obtained during experimentation in presence of external disturbances

TABLE IV: Comparison study

Controllers	Error
Tar*et al.* [19]	± 0.1 Rad
Hyatt *et al.* [20]	–0.0009 Rad
Skorina *et al.* [13]	> 0.1 Rad
Azizkhani *et al.* [16]	0.0721 Rad
Ossaba *et al.* [21]	> 0.1 Nm
MacDonald & Dubay [22]	1.004 N
Proposed controller- method I	0.052 Rad
Proposed controller - method II	0.060 Rad

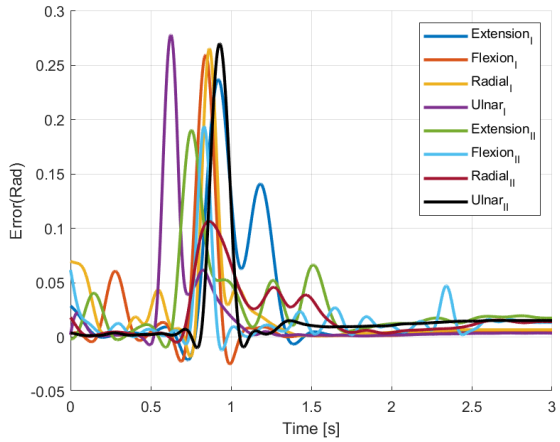

Fig. 37: Errors obtained during experimentation in presence of external disturbances

[35] of a redundant pneumatically actuated soft robot, the trajectory tracking error increased from 2.5 mm in simulation to 4.1 mm in experiments due to actuator delays and external disturbances. Similarly, the tendon-driven extensible soft robot [36] exhibited a simulation error of 3.0 % of its total length, rising to 5.2 % in experiments as a result of tendon slack and stiffness variations. The underwater continuum manipulator demonstrated [37] a 4.8 % spatial deviation in simulation, which increased to 5.0 % when subjected to water currents in real-world testing. The force control error in the environmental contact study [38] grew from 0.35 N in simulation to 0.52 N in experiments, influenced by material compliance and environmental interactions. Lastly, the tendon-driven continuum robot with a non-linear model predictive task-space controller [39] recorded a simulation error of 1.8 mm, increasing to 3.2 mm in experimental trials due to tendon elasticity and external forces. These results consistently show that simulation errors are lower than experimental errors, primarily because real-world uncertainties such as environmental interactions and actuator limitations introduce additional variability in robotic performance.

The errors observed across these studies indicated that simulation results generally exhibit lower deviations compared to experimental trials. This discrepancy is largely due to real-world factors such as actuator delays, environmental disturbances, and material compliance. The underwater manipulator study showed the highest experimental error due to fluid dynamics, while the tendon-driven continuum robot exhibited the lowest simulation error, benefiting from predictive control strategies.

VII. Conclusion and Future Works

The development of an advanced control framework is essential for improving the operational efficiency of soft continuum robots. This study presented an MRAC designed to provide dynamic control over a soft continuum wrist integrated into a prosthetic hand. By leveraging the MRAC methodology and a 4-element parametrized PCC model, the system effectively maintained the desired motion trajectories despite changes in the robot's physical characteristics and external

conditions. The New Theorem of Stability was demonstrated to be a powerful tool for assessing the asymptotic stability of both tracking errors and adaptive parameters, eliminating the need for the uniformly continuous signal condition typically required by Barbalat's lemma. Simulation results showed that the MRAC outperformed both the GVSC and PID controllers in terms of RMSE, settling time, and steady-state errors. The MRAC consistently exhibited lower RMSE, faster settling times, and smaller steady-state errors compared to the other control strategies. However, in experimental trials, the RMSE values were higher than those observed in simulations, primarily due to variations in spring stiffness. Future work will focus on redesigning the wrist structure to improve its robustness and refining the control strategies by integrating real-time sensor feedback to further enhance motion accuracy.

REFERENCES

[1] Palomino-Resendiz, S. I., M. A. Peñaloza-López, D. A. Flores-Hernández, C. U. Solís-Cervantes, and R. L. Palomino-Resendiz. "Model Reference Adaptive Control (MRAC) for dual-axis solar tracker applied in CPV." Solar Energy Materials and Solar Cells 279 (2025): 113225.

[2] C.-C.Hang and P. Parks, "Comparative studies of model reference adaptive control systems," IEEE Trans. Autom. Control, vol. AC-18, no. 5, pp. 419– 428, Oct. 1973.

[3] Lee, Jayden Dongwoo, Lamsu Kim, Kwangwoo Jang, Seongheon Lee, and Hyochoong Bang. "Feedback linearization-based model reference adaptive control for multirotor UAVs under uncertainties from fuel and payload." Proceedings of the Institution of Mechanical Engineers, Part G: Journal of Aerospace Engineering (2025): 09544100241295840.

[4] F. Vasile, E. Maiettini, G. Pasquale, N. Boccardo, and L. Natale, "Continuous Wrist Control on the Hannes Prosthesis: a Vision-based Shared Autonomy Framework," Proc. IEEE Int. Conf. Robot. Autom. (ICRA), May 2025. [Online]. Available: https://arxiv.org/abs/2502.17265

[5] Barkana, Itzhak. "Can stability analysis be really simplified? (revisiting Lyapunov, Barbalat, LaSalle and all that)." (2017).

[6] Zhang, Dan, and Bin Wei. "A review on model reference adaptive control of robotic manipulators." Annual Reviews in Control 43 (2017): 188-198.

[7] M. T. Gillespie, C. M. Best, and M. D. Killpack, "Simultaneous position and stiffness control for an inflatable soft robot," Proceedings - IEEE International Conference on Robotics and Automation, vol. 2016-June, pp. 1095–1101, 2016.

[8] T. W. Chaundy, P. R. Barrett and C. Batey, *The Printing of Mathematics*. London, U.K., Oxford Univ. Press, 1954.

[9] F. Mittelbach and M. Goossens, *The LaTeXCompanion*, 2nd ed. Boston, MA, USA: Pearson, 2004.

[10] Continelli, N. A., Nagua, L. F., Olmos, P. M., Monje, C. A. (2025). Combined model-based and data-driven approach for the control of a soft robotic neck. Robotics and Autonomous Systems, 105155.

[11] Seghiri, T., Ladaci, S., Haddad, S. (2025). Robust Model Reference Adaptive Control Design for 1DOF Flexible Arm with Payload Variations based on Fractional Order MIT Law. WSEAS Transactions on Systems and Control, 20, 227-238.

[12] Huang, X., Rong, Y., Gu, G. (2024). High-precision dynamic control of soft robots with the physics-learning hybrid modeling approach. IEEE/ASME Transactions on Mechatronics.

[13] Skorina, E. H., Luo, M., Tao, W., Chen, F., Fu, J., and Onal, C. D. (2017). Adapting to flexibility: model reference adaptive control of soft bending actuators. IEEE Robotics and Automation Letters, 2(2), 964-970.

[14] Bomfim, M. H. S., Monteiro, N. S., and Lima II, E. J. (2022). Modelling, simulation and implementation of a hybrid model reference adaptive controller applied to a manipulator driven by pneumatic artificial muscles. Robotica, 40(6), 1894-1918.

[15] Hsu, Liu, Ramon R. Costa, Fernando Lizarralde, and Alessandro Jacoud Peixoto. "Arbitrarily Fast Tracking Multivariable Least-squares MRAC." arXiv preprint arXiv:2412.19601 (2024).

[16] Azizkhani, M., Zareinejad, M., and Khosravi, M. A. (2022). Model reference adaptive control of a soft bending actuator with input constraints and parametric uncertainties. Mechatronics, 84, 102800.

[17] Licher, J., Bartholdt, M., Krauss, H., Habich, T. L., Seel, T., & Schappler, M. (2025). Adaptive Model-Predictive Control of a Soft Continuum Robot Using a Physics-Informed Neural Network Based on Cosserat Rod Theory. arXiv preprint arXiv:2508.12681.

[18] Zhou Z, Ai Q, Li M, Meng W, Liu Q, Xie SQ. The Design and Adaptive Control of a Parallel Chambered Pneumatic Muscle-Driven Soft Hand Robot for Grasping Rehabilitation. Biomimetics (Basel). 2024 Nov 18;9(11):706. doi: 10.3390/biomimetics9110706. PMID: 39590278; PMCID: PMC11591751.

[19] Tar, J. K., Kovács, L., Takács, A., Takács, B., Zentay, P., Haidegger, T., and Rudas, I. J. (2014, October). Novel design of a Model Reference Adaptive Controller for soft tissue operations. In 2014 IEEE International Conference on Systems, Man, and Cybernetics (SMC) (pp. 2446-2451). IEEE.

[20] Hyatt, P., Johnson, C. C., and Killpack, M. D. (2020). Model reference predictive adaptive control for large-scale soft robots. Frontiers in Robotics and AI, 7, 558027.

[21] Toro-Ossaba, A., Tejada, J. C., Rúa, S., Núñez, J. D., and Peña, A. (2024). Myoelectric model reference adaptive control with adaptive kalman filter for a soft elbow exoskeleton. Control Engineering Practice, 142, 105774.

[22] MacDonald, I., Dubay, R. (2024). Development of an Adaptive Force Control Strategy for Soft Robotic Gripping. Applied Sciences (2076-3417), 14(16).

[23] Sun, J. (2021). Model Reference Adaptive Control. In: Baillieul, J., Samad, T. (eds) Encyclopedia of Systems and Control. Springer, Cham.

[24] Barkana, Itzhak. "Barbalat's lemma and stability – Misuse of a correct mathematical result?" Journal - MESA 7 (2016): 197-218.

[25] Barkana, Itzhak. "The new theorem of stability and gain convergence in simple adaptive control." (2017).

[26] M. Naeijian and A. Khosravi, "Stability Analysis of Model Reference Adaptive Control with the New Theorem of Stability," 2020 28th Iranian Conference on Electrical Engineering (ICEE), Tabriz, Iran, 2020, pp. 1 − 6, doi: 10.1109/ICEE 50131.2020.9260765.

[27] Sulaiman, S., Gohari, M., Schetter, F., & Ficuciello, F. (2025). A Learning-based Model Reference Adaptive Controller Implemented on a Prosthetic Hand Wrist. arXiv preprint arXiv:2510.19068.

[28] Sulaiman S, Menon M, Schetter F, Ficuciello F. Design, Modelling, and Experimental Validation of a Soft Continuum Wrist Section Developed for a Prosthetic Hand. In2024 IEEE/RSJ International Conference on Intelligent Robots and Systems (IROS) 2024 Oct 14 (pp. 11347-11354). IEEE.

[29] Della Santina C, Katzschmann RK, Biechi A, Rus D. Dynamic control of soft robots interacting with the environment. In2018 IEEEInternational Conference on Soft Robotics (RoboSoft) 2018 Apr 24 (pp. 46-53). IEEE.

[30] M. Letourneau and J. W. Sharp, *AMS-StyleGuide-online.pdf,* American Mathematical Society, Providence, RI, USA, [Online]. Available: http://www.ams.org/arc/styleguide/index.html

[31] H. Sira-Ramirez, "On the sliding mode control of nonlinear systems," *Syst. Control Lett.*, vol. 19, pp. 303–312, 1992.

[32] A. Levant, "Exact differentiation of signals with unbounded higher derivatives," in *Proc. 45th IEEE Conf. Decis. Control*, San Diego, CA, USA, 2006, pp. 5585–5590. DOI: 10.1109/CDC.2006.377165.

[33] M. Fliess, C. Join, and H. Sira-Ramirez, "Non-linear estimation is easy," *Int. J. Model., Ident. Control*, vol. 4, no. 1, pp. 12–27, 2008.

[34] R. Ortega, A. Astolfi, G. Bastin, and H. Rodriguez, "Stabilization of food-chain systems using a port-controlled Hamiltonian description," in *Proc. Amer. Control Conf.*, Chicago, IL, USA, 2000, pp. 2245–2249.

[35] Azizkhani, M., Kousik, S., Chen, Y. (2025). Dynamic task space control of redundant pneumatically actuated soft robot. IEEE Robotics and Automation Letters.

[36] Seleem, I. A., Naeem, M. A., Takemura, H., Ishii, H. (2025). Tendon-driven based extensible soft robot with variable stiffness. Robotics and Autonomous Systems.

[37] Walker, K. L., Chen, H. Y., Partridge, A. J., Cruz da Silva, L., Stokes, A. A., Giorgio-Serchi, F. (2025). Closed-loop control and disturbance mitigation of an underwater multi-segment continuum manipulator. arXiv preprint arXiv:2503.12508.

[38] Dickson, A. K., Pacheco Garcia, J. C., Anderson, M. L., Jing, R., Alizadeh-Shabdiz, S., Wang, A. X., DeLorey, C., Patterson, Z. J., Sabelhaus, A. P. (2025). Safe autonomous environmental contact for soft robots using control barrier functions. arXiv preprint arXiv:2504.14755.

[39] Hachen, M., Shentu, C., Lilge, S., Burgner-Kahrs, J. (2025). A nonlinear model predictive task-space controller satisfying shape constraints for tendon-driven continuum robots. IEEE Robotics and Automation Letters.